HHS Public Access

Author manuscript

Nat Cell Biol. Author manuscript; available in PMC 2022 June 30.

Published in final edited form as:

Nat Cell Biol. 2022 January ; 24(1): 10–23. doi:10.1038/s41556-021-00809-4.

Human alveolar Type 2 epithelium transdifferentiates into metaplastic KRT5+ basal cells

Jaymin J. Kathiriya[1,¶], **Chaoqun Wang**[1,¶,*], **Minqi Zhou**[1], **Alexis Brumwell**[1], **Monica Cassandras**[1], **Claude Le Saux**[1], **Max Cohen**[1], **Kostantinos-Dionysios Alysandratos**[3,4], **Bruce Wang**[1], **Paul Wolters**[1], **Michael Matthay**[1], **Darrell N. Kotton**[3,4], **Harold A Chapman**[1,2,*], **Tien Peng**[1,2]

[1]Department of Medicine, University of California San Francisco, San Francisco, CA 94143

[2]Cardiovascular Institute and Division of Pulmonary, Critical Care, Allergy and Sleep Medicine, University of California San Francisco, San Francisco, CA 94143

[3]Center for Regenerative Medicine, Boston University School of Medicine, Boston, MA 02118

[4]Pulmonary Center and Department of Medicine, Boston University School of Medicine, Boston, MA 02118

Abstract

Loss of alveolar type 2 cells (AEC2s) and ectopic appearance of basal cells in the alveoli characterize severe lung injuries such as idiopathic pulmonary fibrosis (IPF). Here we demonstrate that human alveolar type 2 cells (hAEC2s), unlike murine AEC2s, transdifferentiate into basal cells in response to fibrotic signaling in the lung mesenchyme *in vitro* and *in vivo*. Single cell analysis of normal hAEC2s and mesenchymal cells in organoid co-cultures revealed the emergence of pathologic fibroblasts and basloid cells previously described in IPF. TGFβ1 and anti-BMP signaling in the organoids promoted transdifferentiation. Trajectory and histologic analyses of both hAEC2-derived organoids and IPF epithelium indicated hAEC2s transdifferentiate into basal cells through alveolar-basal intermediates (ABIs) that accumulate in proximity to pathologic *CTHRC1*^{high}/*TGFB1*^{high} fibroblasts. Our study indicates that hAEC2-loss and expansion of alveolar metaplastic basal cells in severe human lung injuries are causally connected through a hAEC2-basal cell lineage trajectory driven by aberrant mesenchyme.

Prior studies in mice have shown that mouse alveolar type 2 cells (mAEC2s) are the resident stem cell population in the alveoli that constitute the entire gas exchange surface

[*]Address correspondence to: Chaoqun Wang, Ph.D., University of California, San Francisco, 513 Parnassus Ave., HSE Building, Room 1350, San Francisco, CA 94143, chaoqun.wang@ucsf.edu, Hal Chapman, M.D., University of California, San Francisco, 513 Parnassus Ave., HSE Building, Room 201, San Francisco, CA 94143, hal.chapman@ucsf.edu.

[¶]Authors contributed equally

Author Contributions

J.J.K., C.W., H.C., and T.P. conceived the experiments and wrote the manuscript. C.W., J.J.K., M.Z., A.B., C.L.S., M.C., B.W., K.A., and performed the experiments, collected samples, and analyzed data. D.N.K., P.W, B.W., M.M. provided materials and input on the manuscript.

The authors declare no competing interest.

of the lung[1, 2]. In idiopathic pulmonary fibrosis (IPF), the most deadly and prevalent form of diffuse parenchymal lung disease, hAEC2s are lost from the alveoli concurrent with the appearance of metaplastic alveolar KRT5+ basal cells that normally appear in the conducting airways[3–9]. Rigorous genetic lineage tracing has shown that metaplastic KRT5+ cells in the murine alveoli are not derived from mAEC2s, but rather from KRT5−/SOX2+ progenitors in the mouse airway after severe alveolar injury from fibrosis or viral infections[5, 6, 10–12]. However, it is not clear whether a similar population in the human airway exists that contributes to metaplastic basal cells, as the airways contain key anatomic differences across the two species[13]. This is a clinically significant question because the extent of alveolar KRT5+ basal cells directly correlates with mortality in IPF[14]. In this study, we made a surprising finding that hAEC2s, but not mAEC2s, can readily transdifferentiate into KRT5+ basal cells in organoid culture and xenotransplant. Moreover, we define pro-fibrotic mesenchymal niche-derived factors that promote hAEC2-to-basal cell transdifferentiation. Finally, quantitative spatial analysis of IPF lung tissue reveals basal cells and advanced alveolar-basal intermediates are surrounded by aberrant, CTHRC1^{hi} pro-fibrotic mesenchyme. These results identify hAEC2s as a source of metaplastic KRT5+ basal cells in severe alveolar injuries, and provide a potential explanation for the reported appearance of aberrant hAEC2s with basaloid features in the transcriptomes of IPF and other severe lung injures such as COVID pneumonia (cite)[8, 9].

RESULTS

hAEC2s transdifferentiate into basal cells *in vitro*

Previously reported hAEC2 organoids have utilized MRC5, a fetal human lung fibroblast cell line, as feeders to maintain primary adult hAEC2s *in vitro,* at least in part through local BMP and Wnt signaling[1,15]. We confirmed similar organoid development using low passage MRC5 cells in our 3D organoid system and hAEC2s isolated with the HTII-280 antibody (EpCAM+/HTII-280+) (Fig. 1b,c, Extended Data Fig. 1a), with high purity of hAEC2 confirmed by single cell RNAseq (scRNAseq) and cytospin (Fig. 1a and Extended Data Fig. 1b,c). We hypothesized that primary mesenchyme obtained from normal adult lungs would provide a more supportive niche. We used a flow cytometry strategy to isolate adult human lung mesenchyme (AHLM) (CD45−/CD11b−/CD31−/EpCAM−) that was previously described by scRNAseq to yield a predominantly PDGFRα+ fibroblast population[16] (Extended Data Fig. 1d), and co-cultured AHLM with hAEC2 in 3D organoid. While there was no difference in colony-forming capacity between MRC5 and AHLM, we saw a dramatic loss of SFTPC accompanied by gradual appearance of KRT5, an airway basal cell marker, in hAEC2 organoids co-cultured with AHLM (Fig. 1d,e) (Extended Data Fig. 1e). By day 14 of co-culture, the majority of the organoids derived from hAEC2-AHLM co-culture contained KRT5+ cells, whereas the majority of organoids in the hAEC2-MRC5 co-cultured contained only SFTPC+ cells (Fig. 1c,e). Further immunophenotyping of KRT5+ organoids from hAEC2 co-cultured with either AHLM or MRC5 demonstrated that most KRT5+ cells arising from MRC5 co-culture do not stain for other mature basal cell markers such as TP63 or KRT17 (Extended Data Fig. 1f,h), whereas the majority of KRT5+ cells derived from AEC2/AHLM organoids are also TP63+ and KRT17 (Extended Data Fig. 1g,h). Some of the organoids assume apical-basal polarity with KRT5+ basal cells

in the outer layer, and KRT5−/KRT8+ cells in the inner layer (Extended Data Fig. 1i), which have been identified as a transitional cell type derived from AEC2s[17–20]. To further ensure that the basal cells did not result from an outgrowth of contaminants in the HTII-280 sort, we cultured hAEC2 in previously defined mesenchymal-free, alveolar growth media[21] over a month to enrich for hAEC2s (cytospin shows >99% purity) prior to coculture with AHLM, which resulted in the same basal cell differentiation as seen with freshly isolated hAEC2s (Extended Data Fig. 1k). Comparison of hAEC2 organoids utilizing passage 0 (freshly sorted) vs. passage 2 from the same AHLM donor did not show any significant difference in KRT5 transdifferentiation (Extended Data Fig. 1j). A parallel experiment using murine AEC2s (mAEC2s) co-cultured with primary adult murine lung mesenchyme (AMLM) under identical *in vitro* conditions produced no KRT5+ organoids (Extended Data Fig. 2a,b). Conversely, culturing hAEC2 with AMLM failed to generate organoids (Extended Data Fig. 2c).

To further study the capacity of hAEC2s to differentiate into KRT5+ basal cells using a trackable differentiation system, we utilized a previously validated human induced pluripotent stem cell-derived AEC2 (iAEC2) model system[22]. We generated stably self-renewing iAEC2s in epithelial-only (feeder-free) cultures from the published SPC2-ST iPSC line that has been previously engineered with a tdTomato reporter targeted to one allele of the endogenous *SFTPC* locus to isolate iAEC2s lacking basal cell transcripts[23]. As previously shown, we confirmed purity of iAEC2s as judged by the absence of basal cell markers and maintenance of robust tdTomato expression (Fig. 1f). Next, we co-cultured iAEC2s with either MRC5 or AHLM in our previously published media that has been optimized to maintain iAEC2 fate in culture[22, 23] (CHIR, KGF, dexamethasone, cyclic AMP, and IBMX, hereafter called CK/DCI). In stark contrast to iAEC2 co-cultured with MRC5, iAEC2 co-cultured with AHLM dramatically lost *SFTPC* expression as evidenced by the loss of tdTomato fluorescence (Fig. 1g). Immunophenotyping confirmed the loss of SFTPC in iAEC2 co-cultured with AHLM in virtually all organoids, along with the emergence of intermediate and early basal cell markers KRT8 and KRT17, respectively in approximately 65% of organoids (Fig. 1i,j). Interestingly, iAEC2s co-cultured with AHLM do not completely transdifferentiate into KRT5+ basal cells in CK/DCI. Further experiments revealed CHIR as the main media component that prevents basal cell differentiation (Extended Data Fig. 2d,e) and when CHIR was reduced by dilution there was complete differentiation into basal cells that are also positive for KRT5, KRT14, and p63, while retaining NKX2–1, confirming lung fate (Fig. 1k,l, Extended Data Fig. 2f).

hAEC2 transdifferentiate to basal cells in a fibrotic host *in vivo*

Prior transplant study of freshly sorted murine AEC2s demonstrate no evidence of basal cell transdifferentiation when engrafted in injured lungs[24]. To determine whether *in vitro* transdifferentiation capacity of hAEC2s is maintained *in vivo*, we transplanted freshly sorted hAEC2s into bleomycin-induced fibrotic lungs of NSG mice on day 10 (Fig. 2a). hAEC2s were transplanted either alone or with MRC5 or AHLM cells, analogous to ex vivo experiments with 3D organoids. Using the human-specific nuclear antigen (HNA), we were able to identify numerous patches of human cells predominantly in damaged alveolar regions 10 days after transplant (D20 post bleomycin injury). Co-staining with

KRT5 identified HNA+/KRT5+ cells that were SFTPC− where the metaplastic basal cells appeared to form “bronchiolized” cysts in the murine host (Fig. 2c). Utilizing an antibody specific to human-pro-SP-C, we also noted the presence of HNA+/pro-SP-C+ hAEC2 patches in the lung that were spatially distinct from dysplastic basal patches (Fig. 2b,c). Immunohistology analysis showed that when transplanted alone or with MRC5 cells, the majority of the hAEC2s retained alveolar fate (~75%) whereas co-transplants of a similar AHLM:AEC2 ratio resulted in a majority of the patches comprised of KRT5+ basal cells (~80%) (Fig. 2b,c). To determine whether transplanted AHLM and hAEC2s are associated in fibrotic lung, we labeled AHLM with a lentivirus expressing RFP followed by co-transplantation of hAEC2s and RFP-labeled AHLM. Interestingly, we found pods of hAEC2s with basaloid feature (SFTPC+/KRT5+/HNA+, green arrows) along with basal cells (SFTPC−/KRT5+/HNA+, green arrows) in regions adjacent to engrafted RFP+ AHLM (Fig. 2d, orange arrows). We also detected clusters of cells co-expressing AEC2 (SFTPC), basal (KRT5), and transitioning (KRT8)[17, 19] cell markers, adjacent to AHLM (Fig. 2e). The xenotransplantation experiments demonstrate that hAEC2s are capable of reconstituting a fibrotic milieu *in vivo* and transdifferentiate into basal cells with high efficiency in the presence of AHLM, confirming the in vivo plasticity of hAEC2s.

IPF-like mesenchymal subsets emerge during AHLM culture

hAEC2 co-cultured with IPF mesenchyme accelerated basal cell transdifferentiation compared to passage-matched AHLM from normal donors (Extended Data Fig. 3a,b). To determine whether AHLM acquire features of IPF mesenchymal subsets with culture, we analyzed scRNAseq of fresh (sorted from donor lung, uncultured) AHLM (normal donors, N = 3), fresh IPF mesenchyme (N = 3), and cultured AHLM at passage 0–1 isolated from organoids (N = 2). IPF lungs were collected from patients undergoing lung transplantation, and AHLM collected from cadaveric donors without prior history of lung disease. Library preparation was performed separately and mesenchymal cells were segregated based on *PDGFRA* expression, and merged for UMAP and clustering into distinct mesenchymal subsets (Fig. 3a). UMAP analysis showed fairly consistent clustering of subsets across AHLM and IPF donors respectively (Extended Data Fig. 3c). Fresh AHLM consists mainly of proximal (advential, labeled as prox 1, 2), and distal (alveolar) fibroblasts[16] along with a small population of smooth muscle (SM) (Fig. 3c). However, cultured AHLM underwent a dramatic shift in cellular identity, with the loss of distal alveolar fibroblast identity similar to IPF mesenchyme (Fig. 3c, **blue box,** Supplementary Table 1). Instead, a *CTHRC1*-high (*CTHRC1*^{hi}) fibroblast cluster, and a separate *HAS*-high (*HAS*^{hi}) cluster in emerged in cultured AHLM that was rare in fresh AHLM but enriched in IPF (Fig. 3b,c, **red boxes,** Supplementary Table 1). The merged UMAP demonstrated a clear overlap in identities of the *CTHRC1*^{hi} and *HAS*^{hi} fibroblast subsets derived from fresh IPF and cultured AHLM (Fig. 3c). The emergence of these new subsets in culture was very interesting because both *HAS*^{hi} [8] and *CTHRC1*^{hi} [25] fibroblast subsets have been previously identified as fibroblast subsets in single cell analysis of IPF lungs. Analysis of differentially expressed genes demonstrated highly concordant marker expressions in the pathologic mesenchymal niche subsets in cultured AHLM and IPF mesenchyme (Fig. 3d, Extended Data Fig. 3d, Supplementary Table 1). Both *CTHRC1*^{hi} and *HAS*^{hi} subsets arising in cultured AHLM and IPF display features of fibrotic transformation. The *CTHRC1*^{hi} fibroblast subset is

characterized by high expression of collagen along with *TGFB1* (Fig. 3b,d,e), and the *HAS*^{hi} fibroblast subset is characterized by the elevated expression of secreted BMP antagonists that have previously been shown to be elevated in IPF lungs[26] (Fig. 3b,d,f). Analysis of immune subsets in IPF lungs shows that *TGFB1* is also highly expressed in the macrophage population found in fibrotic lungs (Extended Data Fig. 3e–g). This analysis shows that pathologic fibroblast subsets emerge from cultured AHLM that are present in IPF, and they express niche factors that could potentially promote metaplastic transdifferentiation of hAEC2 into basal cells.

Pathological niche signaling modulates transdifferentiation

To further define niche factors promoting hAEC2 transdifferentiiation, we examined the transcriptome of cultured AHLM vs. MRC5 by bulk RNAseq. Differentially expressed gene (DEG) analysis shows significant upregulation of multiple secreted BMP antagonists in the AHLM along with TGFβ ligands, whereas BMP ligands and hedgehog antagonist, *HHIP*, were preferentially upregulated in MRC5 (Fig. 4a, Supplementary Table 2). HHIP is a secreted antagonist of SHH that has previously been identified in both human hAEC2s and mesenchymal niche cells[27], and its expression is reduced in IPF[8]. Hedgehog (Hh) activation can manipulate BMP signaling to modify basal cell metaplasia in murine models[26], and addition of recombinant HHIP to hAEC2 organoids co-cultured with AHLM significantly attenuated *KRT5* expression while increasing *SFTPC* expression in the organoids (Fig. 4b), which is confirmed by immunophenotyping of organoid sections (Fig. 4c). HHIP treatment attenuated expression of Hh transcriptional activator, *Gli1*, in AHLM cocultured with hAEC2s, concurrent with an increase in the expression of BMP ligands (Fig. 4d). Similar to HHIP, addition of recombinant BMP4 significantly attenuated hAEC2 transdifferentiation into basal cells (Fig. 4e,f) and other airway lineages such as club cells (Extended Data Fig. 4a). Conversely, addition of DMH1, a small molecule inhibitor of BMP activation, and recombinant TGFβ1 both augmented the number of basal cells derived from hAEC2s cocultured with MRC5 (Fig. 4g,h). This demonstrates that active TGFβ signaling promotes hAEC2 transdifferentiation into basal cells while BMP activation in the hAEC2 niche maintains AEC2 fate, which could account for the differential effects of AHLM vs. MRC5 in their ability to promote basal cell differentiation.

hAEC2-derived basal cells resemble IPF metaplastic basal cells

There is increased recognition of basal cell heterogeneity in normal and diseased lungs, with specific basal cell subsets increased in IPF[28]. To compare hAEC2-derived basal cells in organoids with basal cells isolated from intact lungs, we analyzed scRNAseq of freshly isolated epithelial cells isolated from distal fragment (not from trachea) of normal donor lungs (N = 2), IPF lungs (N = 2), and hAEC2-derived basal cell isolated from organoids (N = 2). Library preparation was performed separately, basal cells were segregated based on *KRT5* expression, and merged for UMAP and clustering into distinct basal subsets (Fig. 5a, Extended Data Fig. 5a). Clustering revealed four distinct subsets of basal cells with high degree of gene overlap with previously identified basal cell subsets in vivo[28], including secretory primed (SPB), multipotent (MPB), activated (AB), and proliferating (PB) (Fig. 5a–c, Extended Data Fig. 5b). Interestingly, the plurality of hAEC2-derived basal cells are secretory primed basal cells (Fig 5a, Extended Data Fig. 5c, **red box**), a population that

was identified as the predominant basal population in the alveoli of IPF lungs[28]. Basal cell subset-specific marker analysis shows similarities in expression of genes in hAEC2-derived and IPF basal cells (Fig. 5c).

To explore further whether IPF biomarkers are upregulated in hAEC2-derived basal cells, we performed DEG analysis comparing basal cells from normal lung vs. hAEC2-derived basal cells. This analysis showed that while hAEC2-derived basal cells express similar canonical basal markers such as *SOX2*, *NGFR* and *TP63*, they over-express markers previously reported to be upregulated in IPF epithelium, such as *KRT14, VIM*, and *MMP7*[3, 4, 8, 9, 29] (Fig. 5d). Histologic comparison of normal lungs, IPF lungs, and hAEC2-derived organoids shows that these IPF biomarkers are preferentially present in basal cells from IPF and hAEC2-derived organoids, but not normal lungs (Fig. 5e). Finally, to identify common gene signature of IPF and hAEC2-derived basal cells, we performed an overlap analysis of DEGs of IPF basal cells and hAEC2-derived basal cells compared with normal lung basal cells. Hypergeometric probability testing shows significant enrichment of overlap genes in DEGs between hAEC2-derived and IPF basal cells (Extended Data Fig. 5d), generating a large list of DEGs that were shared between IPF and hAEC2-derived basal cells (Extended Data Fig. 5e, Supplementary Table 3). These results demonstrate that while hAEC2-derived basal cells express canonical basal cell gene programs, they share more similarities with IPF basal cells ectopically localized in the diseased alveoli.

hAEC2s to basal cells occurs through intermediate states.

Recently, AEC2-derived intermediate cell types have been described in the alveolar space of bleomycin-challenged mice and IPF lungs[8, 9, 17, 19]. To determine whether we observe similar discrete intermediates in the progressive transdifferentiation of hAEC2s toward basal cells in organoids, we analyzed the time course of all epithelial cells (based on *EPCAM* expression) undergoing transdifferentiation *in vitro* by scRNAseq. Epithelial cells from D0 (live sort of HTII-280+ prior to culture, Fig. 1a and Extended Data Fig. 1a, b), D7 (7 days after co-culture), D14, and D21 organoids were sequenced separately, then merged and clustered by uniform manifold approximation and projection (UMAP) where 6 main clusters emerged (Fig. 6a, Extended Data Fig. 6a, Supplementary Table 4). Four clusters were easily identified by lineage markers of hAEC2s, basal cells, club cells, and ciliated cells respectively (Extended Data Fig. 6a,c,d). Time course shows a time-dependent loss of the hAEC2 population and gain of *KRT5*+ basal cell population, along with an early emergence of two distinct alveolar-basal intermediates (ABIs) bearing both hAEC2 and basal markers at D7 that recedes with time in culture (Fig. 6a, highlighted by dotted line). ABI1 cells are identified by persistence of *SFTPC, ABCA3*, and *NAPSA*, along with the emergence of *KRT17* (Fig. 6i, Extended Data Fig. 6e). ABI2 cells are identified by low levels of AEC2 markers, higher levels of KRT17, and absence of KRT5 (Fig. 6i, Extended Data Fig. 6e). Both these intermediates express high levels of KRT8 (Fig. 6i, Extended Data Fig. 6i), a marker of intermediate cell types described earlier[17, 19]. Of note, we observed a SFTPClow/KRT8+/KRT5− population comparable to ABIs in the epithelial cells derived from hAEC2s in vivo after engraftments in mice. (Fig. 2d). Concurrent with the disappearance of the ABIs over time, there is also a progressive emergence of SCGB1A1+ club cells and FOXJ1+ ciliated population in culture (Fig. 6a, Extended Data Fig. 6c,d),

suggesting that transdifferentiated KRT5+ cells are mature basal cells capable of further differentiation into club and ciliated lineages.

The emergence of ABI1 and ABI2 intermediate populations in the direct line of transdifferentiation to basal cells was confirmed by both Monocle and RNA trajectory analysis (Fig. 6b–d). Visualization of gene expression along the hAEC2 transdifferentiation trajectory shows that well-established AEC2 marker, *LAMP3,* and new hAEC2 marker, *HHIP27*, are quickly lost first as mature hAEC2s transition into ABIs (Fig. 6c, Extended Data Fig. 6a,b). The emergence of early basal marker, *KRT17*, and transitional-state marker, *KRT8*[17–20], concurrent with the persistence of AEC2 markers *SFTPC*, *ABCA3*, and *NAPSA*, marks the ABI1 populations seen early in culture (Extended Data Fig. 6b–d). The presence of the ABI1 and ABI2 is confirmed on immunophenotyping of D7 organoids early in the transdifferentiation, where we see KRT17−/KRT8+/SFTPC+ and KRT17+/KRT8+/SFTPC^{low} cells, in addition to a minority of organoids (9%) that contains only completely transdifferentiated into basal cells (KRT17+/KRT5+) (Fig. 6e). As transdifferentiation progresses, the ABIs give away to mature basal cells as all hAEC2 markers are lost with the emergence of mature basal cell markers *KRT5* and *KRT14* (Fig. 6c,i, Extended Data Fig. 6a,e,i). An upstream IPA analysis of pathways driving hAEC2s, ABI1 and ABI2s confirmed the distinct expression profiles of these intermediates. ABI1 cells exhibited active upstream drivers typical of hAEC2s (FOXA2, GATA4, NKX2–1) relative to ABI2s (Fig. 6f). Conversely, the ABI2s are preferentially activated by basal cell pathways (TP63, HES1, SOX2) along with TGFβ1 signaling and expression of mesenchymal markers (Fig. 6f, Supplementary Table 5).

Identification of AEC2 to basal cell ABIs in fibrotic human lungs

Several recent studies in mice have reported mAEC2s undergo a transitional state when differentiating into mAEC1s *in vitro* and *in vivo*[18–20]. The pre-alveolar type 1 transitional cells (PATS) described in mouse[20] were equated with both the transitional AEC2s and KRT17+/KRT5− basaloid cells described earlier[8, 9] and labeled as “PATS-like cells” in human. However, basal cells were omitted from the original analysis[20] even though the KRT17+/KRT5− basaloid cells express low levels of canonical basal cell transcription factor *TP63* (Habermann *et al*[8] and Kobayashi *et al*[20]). Therefore, we hypothesized that PATS-like cells, inclusive of transitional AEC2s and KRT17+/KRT5− basaloid cells, also represent intermediate cells between AEC2s and basal cells. To this end, we re-analyzed IPF epithelial transcriptomes to include basal cells from the original dataset (from Haberman *et al*[8], analyzed by Kobayashi *et al*.[20]), and then performed Monocle trajectory analysis (Fig 6g, h). This analysis confirmed an hAEC2-hAEC1 trajectory through transitional AEC2s. However, inclusion of basal cells in the analysis also revealed an equally prominent hAEC2 to basal cell trajectory through the KRT17+/KRT5− basaloid cells (Figure 6g, h). We then directly compared the genes found to be upregulated in PATS-like cells in IPF[20] with the organoid ABIs (ABI1 and ABI2) and observed an almost identical expression pattern (Fig. 6i, Extended Data Fig. 6f–i). The organoid ABI1 population appears similar to the transitional AEC2s while the organoid ABI2 population appears similar to the KRT17+/KRT5− basaloid cells (Fig. 6i). Together these findings suggest that ABIs derived from hAEC2s in our 3D organoid culture recapitulate previously identified intermediate cell populations in IPF lungs

and suggest a direct trajectory from hAEC2s to basal cells through these intermediate cell types.

Consistent with our *in silico* prediction of a continuous trajectory from hAEC2s to ABIs to basal cells, we found evidence of all four cell types in the same cystic region (Fig. 7a, Extended Data Fig. 7a) as judged by protein staining for hAEC2s (SFTPC+/KRT8^{low}/KRT17−/KRT5−), ABI1 (SFTPC+/KRT8^{hi}/KRT17^{low}/KRT5−), ABI2 (SFTPC^{low}/KRT8^{hi}/KRT17+/KRT5−), and basal cells (SFTPC−/KRT8−/KRT17+/KRT5+). Furthermore, ABI2s can be subdivided based on the presence of TP63, as we found several examples of both TP63+/KRT17+/KRT5− and TP63−/KRT17+/KRT5− ABI2s in the lungs of IPF patients (Extended Data Fig. 7a), comparable to previously described basaloid (KRT17+/KRT5− cells that are either TP63+ or TP63−) populations in IPF[8, 9, 20]. Next, we systematically inspected IPF lungs for the presence of ABIs by RNA *in situ* hybridization as a function of the extent of alveolar remodeling using a combination of markers for ABI1, ABI2, and basal cells, all of which express varying levels of *KRT17* mRNA. As expected, ABI1 or ABI2 were extremely rare in the alveolar regions of normal lung (Extended Data Fig. 7b). Considering the highly heterogeneous histology of an IPF lung, we focused our analysis of ABIs in histologically defined regions (Fig. 7b). The relative frequencies of ABI1s and ABI2s correlated with progression of disease. In the normal-appearing and thickened alveolar regions of IPF lungs reflecting histological regions of minor injury, >80% of the *KRT17+* cells were SFTPC+ ABI1s while the remaining were *KRT17*+/*SFTPC*−/KRT5− ABI2s (Fig. 7c). Conversely, in areas of moderate to severe injury reflected by presence of microcystic regions, the majority of *KRT17+* cells were ABI2s (63%) and with emergence of a small number of *KRT17+*/KRT5+ basal cells (10% of KRT17+ cells)(Fig. 7c). Finally, in areas with complete bronchiolization and heavy fibrosis, we found few ABI1s (2%) and ABI2s (30%) with 68% of KRT17+ cells now acquiring complete basal identity as judged by KRT5 expression (Fig. 7c). Furthermore, by immunostaining we found evidence of ABIs in lungs with scleroderma and COVID-19 showing linearly connected AEC2s (SFTPC+), ABI1s (SFTPC+/KRT17+), ABI2s (SFTPC−/KRT17+/KRT5−), and basal cells (KRT17+/KRT5+) cells in the same area of the disease lung (Fig. 7d, Extended Data Fig. 7c). The results strongly suggest that ABI populations *in vivo*, similar to the population identified in our 3D organoids, appear as a function of alveolar injuries that result in transdifferentiation of hAEC2 to basal cells.

Analysis of AHLM cocultured with hAEC2s in our organoid platform identified a *TGFB1*^{hi} mesenchymal population that is marked by *CTHRC1* gene expression, which has been shown previously to be associated with fibroblastic foci[25]. Because ABI2s have elevated TGFβ signaling (Fig. 6f), that can antagonize BMP signaling[30, 31], we tested the hypothesis that aberrant mesenchyme providing a profibrotic *TGFB1*^{hi} niche is spatially associated with ABIs. We probed IPF lung specimens in situ with ABI markers (*SFTPC* and *KRT17*) and profibrotic mesenchymal marker *CTHRC1*, followed by protein staining for basal marker KRT5 (Fig. 8a). Consistent with our hypothesis, while ~10% of ABI1s were adjacent to *CTHRC1*+ cells, 83% of ABI2s were found adjacent to *CTHRC1*+ mesenchyme, suggesting a high degree of association between metaplastic intermediate cells and TGFβ1^{hi} profibrotic mesenchymal cells (Fig. 8b). We also found that *CTHRC1*+ mesenchyme was also associated with 77% of all basal cells found in actively remodeling regions (Fig. 8b).

These data indicate that hAEC2s transdifferentiate into metaplastic basal cells through a series of intermediates, at least in part in a fibrotic niche made of TGFβ1^{hi}, pro-fibrotic mesenchymal populations (Fig 8c).

DISCUSSION

There is currently an assumption that the regenerative capacity of AEC2s, the resident stem cell of the alveolus, is highly conserved between mouse and human[32]. However, the unexpected finding that unlike mAEC2s, hAEC2s robustly transdifferentiate into functional basal cells with cues from pathological mesenchymal cells arising *in vitro* invited the possibility that a parallel process occurs in human diseases characterized by severe alveolar injuries *in vivo* (*e.g.* IPF and COVID). Single cell analysis of the cultured mesenchymal niche cells responsible for the transdifferentiation (AHLM) demonstrated the emergence of two fibroblast subpopulations recently identified in freshly isolated IPF lungs that are enriched in either secreted TGFβ1 (*CTHRC1*^{hi}) or BMP antagonists (HAS^{hi}). Similarly, single cell analysis of the hAEC2-to-basal cell trajectory *in vitro* revealed the presence of intermediate cell types and basal cell subsets previously identified in IPF lungs. These findings validate our AHLM/hAEC2 organoid assay as an *in vitro* model for hAEC2-mesenchymal crosstalk that results in stem cell metaplasia seen in severe alveolar injury, and provides experimental confirmation of a stem cell trajectory that is seen in diseased human, but not murine lung.

Another group of recent studies have also identified an intermediate cell-state between AEC2 to AEC1 differentiation, first described in mice, that is marked by elevated expression of KRT8 and increased TGFβ1 signaling[17, 19, 20]. These murine intermediate cell types bear striking resemblance to the human ABIs identified in our study, suggesting that a KRT8 high intermediate state may not be unique during AEC2-to-AEC1 transdifferentiation in mice, but also evolved to include AEC2-to-Basal transdifferentiation in human. Furthermore, ABI1 and ABI2 found *in vitro* are remarkably similar to discrete intermediate cell types, *i.e.* transitional AEC2s and KRT5−/KRT17+ aberrant basaloid cells, described in IPF lungs. A comparative IPA analysis of hAEC2, ABI1, and ABI2 transcriptomes (Fig. 6f) reveals the extensive transcriptional reprogramming involved in the transdifferentiation through these intermediate states, including progressive loss of AEC2-promoting signaling, such as NKX2–1, and the emergence of numerous activities promoting mesenchymal features, especially the strong activation of TGFβ1 signaling in ABI2s. We focused on TGFβ1 because TGFβ1 promotes hAEC2 transdifferentiation to basal cells in organoids, and *CTHRC1*^{hi} fibroblasts known to be *TGFB1*^{hi} emerge both in our organoid assay and in IPF tissues. Indeed, over 80% of the ABI2 clusters and 67% of alveolar basal cells were found adjacent to *CTHRC1*^{hi} fibroblasts (Fig 8). These spatial relationships are consistent with high TGFβ1 signaling observed as an upstream driver of ABI2 signaling (Fig. 6f).

That hAEC2s undergo progressive transdifferentiation to metaplastic basal cells is not unique to IPF. Alveolar metaplastic basal cells are also common in sections of scleroderma and COVID lungs, and these are intermingled with ABI1 and ABI2 intermediates in areas of active remodeling (Fig. 7d). The common finding of ABIs in hAEC2-derived organoids as well as hAEC2 xenografts, and in histologic analyses of fibrotic lungs suggest hAEC2s

are a major source of metaplastic basal cells in diseases with severe alveolar injury. Future studies are needed to clarify if and under what circumstances hAEC2 reprogramming toward metaplastic basal cells in the alveoli is reversible, and whether other components of the fibrotic niche such as endothelial cells and immune cells are able to drive the metaplastic phenotype.

METHODS

This study complies with all relevant ethical regulations that are approved by UCSF Institutional Review Board (IRB) and Institutional Animal Care and Use Committee (IACUC).

Human Lung Tissue

Studies involving human tissue were approved by the UCSF Institutional Review Board. All subjects provided written informed consent. Peripheral regions of the normal lungs were obtained to select for distal most regions of the lung from brain-dead donors that were rejected for lung transplantation. IPF, scleroderma, and ARDS (COVID19) lung specimens were taken from the periphery of the lung at the time of lung transplant. Age and sex of tissue donors are listed in Supplementary Table 6.

Animal Studies and Treatment

Mice were housed in accordance with UCSF IACUC protocol in humidity- and temperature-controlled rooms on a 12 h light-dark cycle with free access to food and water. 8–12 weeks old animals were used for the experiments. For labeling mAEC2s, *Sftpc*$^{creERT2/+}$:*R26R*$^{mTmG/+}$ mice[33, 34] were intraperitoneally administered with tamoxifen (Cat#T5648; Sigma) at 200 mg/kg weight per day for three consecutive days. NOD.Cg-*Prkdc*^{scid} *Il2rg*^{tm1Wjl}/SzJ (NOD *scid* gamma; NSG) mice were previously described[35, 36]. Animal studies utilized a minimum of 4 mice per group. Mice were injured with oral aspiration of bleomycin (2.1 U/kg body weight). Mice were weighed twice a week. Mice were sacrificed between Day 17–20 post injury for histopathological analysis.

Histology and Immunofluorescence

Paraffin Embedding: Mouse lungs were inflated with and fixed in 4% paraformaldehyde (PFA) overnight at 4 °C. Human lung pieces were fixed in 4% PFA overnight at 4 °C. The lungs were then washed with PBS 4 times for 30 mins each at 4 °C, and then dehydrated in a series of ethanol (30%, 50%, 70%, 95%, and 100%). The dehydrated lungs were incubated with xylene for 1 hr at RT and then embedded in paraffin. The lungs were sectioned at 8 μm on a microtome.

OCT Embedding: 94%OCT/2%PFA/4%PBS-inflated lungs were fixed with 4% PFA for 1 hr at RT, washed with PBS for 4 hrs at RT, and embedded in OCT after 30% and 15% sucrose gradient washing. Organoids in 3D matrigel were fixed with 4% PFA for 30 mins at RT or overnight at 4 °C, then washed in PBS overnight 3X, followed by embedding in OCT. 8 μm sections were cut on a cryostat.

Immunofluorescent staining: Paraffin sections were incubated in xylene for 10 mins twice, then rehydrated in ethanol washes (100%, 95%, 70%, 50% ethanol) for 5 mins each. OCT embedded slides were fixed in 4% PFA at RT for 10 mins, then washed with PBS. For both paraffin and OCT embedded slides, antigen retrieval (Cat#DV2004MX; Biocare) was performed for 30 mins at 95 °C or at 155 °C followed by incubation with sodium borohydride (Sigma) in PBS. Slides were washed with 0.1% Tween-20 in PBS (PBST), blocked (3% donkey serum in PBST) for 1 hr, and then incubated with primary antibodies overnight at 4 °C. The following primary antibodies were used: anti-SFTPC (Cat#AB3786; Millipore; 1:2000), anti-SFTPC (Cat#sc-518029; Santa Cruz; 1:100), anti-KRT5 (Cat#905901; BioLegend; 1:500), anti-KRT14 (Cat#CBL197; Millipore; 1:200), anti-KRT17 (Cat#sc-393002; Santa Cruz; 1:100), anti-p63 (cat#13109; CST; 1:100), anti-KRT8 (cat#TROMA-I; DSHB; 0.045 μg/mL), anti-LAMP3 (cat#AF0487; R&D; 1:200), anti-ABCA3 (Cat#ab99856; Abcam; 1:500), anti-human nuclear antigen (Cat#ab86129; Abcam; 1:500), anti-MMP7 (Cat#MAB3315; Millipore; 1:200), anti-Ac-Tuba1a (Sigma; Cat#T7451, 1:500), anti-p-SMAD1/5/8 (Cat#AB3848-I; Millipore; 1:100), anti-beta IV Tubulin (Abcam; Cat#ab11315; 1:200), and anti-SCGB1A1 (R&D; Cat#MAB4218; 1:500). Slides were washed with PBST and then incubated with secondary antibodies for 1 hr at RT. The following secondary antibodies were used at 1:250: anti-chicken IgY (H+L) AF647 (Jackson ImmunoResearch; Cat# 703–605-155), anti-rabbit IgG (H+L) AF555 (Thermo Fisher; Cat# A-31572), anti-rabbit IgG (H+L) AF488 (Thermo Fisher; Cat# A-21206), anti-mouse IgG (H+L) AF555 (Thermo Fisher; Cat# A-31570), and anti-rat IgG (H+L) AF488 (Thermo Fisher; Cat# A-21208). DAPI was added for 5 mins, and slides were then mounted. Images were captured using Zeiss Imager M1 and analyzed using Axiovision 4.8.2 or Zeiss ZEN v3.1 (Zeiss, Germany). Where indicated, multiple images at 20X were captured using the “MosaiX” function and stitched together using “Tile Stitch” function in the Axiovision or ZEN. Final images were prepared in affinity designer v1.10.1.1142.

Organoid composition calculation: An organoid constituted of SFTPC+ cells and no KRT5+ cells was counted as an alveolar organoid (SFTPC+), an organoid constituted of both SFTPC+ and KRT5+ cells was counted as a hybrid organoid (SFTPC+/KRT5+) and an organoid constituted of KRT5+ cells and no SFTPC+ cell was counted as a basal organoid (KRT5+). Organoids with no detectable staining of either SFTPC or KRT5 were counted as unstained organoids (SFTPC−/KRT5−). To characterize and compare basal cells derived from AEC2/MRC5 and AEC2/AHLM co-cultures, organoids were harvested and stained at D14 with basal cell markers. Individual KRT5+ cells were counted for protein expression of other basal markers and represented as a percentage of total KRT5+ cells. Day 7 organoids and for testing the effects of BMP4, HHIP, CHIR, KGF, TGFβ1, and DMH-I on transdifferentiation of hAEC2 into KRT5+ basal cells, the percentage of SFTPC+, KRT5+, SFTPC+/KRT5+ cells, and ABIs were calculated by counting all the cells across multiple organoids on at least one slide.

Lung digestion and fluorescence activated cell sorting (FACS)

Human lung pieces were washed in PBS (2x) and HBSS (1x) for 10 mins at RT, compressed to remove liquid, and dissected into 1 cm^3 pieces. 15 U/ml Dispase II (Cat#17105041; Thermo fisher), 225 U/mL Collagenase Type I (Cat#17100017; Thermo Fisher), 100 U/mL

Dnase I (Cat#DN25; Sigma-Aldrich), and 1% pen/strep in 1X HBSS were used to digest the pieces for 2 hrs at 37°C. Fungizone (1:400) was added for the final 30 mins of the digestion. The digested tissue was liquified in a blender. The suspension was serially filtered through gauze, 100 μm, 70 μm, and 40 μm strainers. Red blood cells were removed using Red Blood Cell Lysis Buffer (Sigma). After Fc blocking, immune and endothelial cells were depleted using biotinylated CD45 (Cat#368534; BioLegend, 1:200), CD31 (Cat#13–0319-80; eBioscience; 1:200), and CD11b (Cat#301304; BioLegend; 1:200) antibodies and running through streptavidin beads (Cat#17663; STEMCELL Technologies) at 25 μl/ml. The following antibodies were used at 1:200: anti-CD45-APC-Cy7 (BioLegend; Cat#304014), anti-CD11b-APC-Cy7 (BD; Cat#557754), anti-CD31-APC-Cy7 (BioLegend; Cat#303120), anti-CD326-PE (BioLegend; Cat#324206), anti-HTII-280 (Terrace Biotech, Cat#303118), and anti-mouse IgM-AF488 (Cat# A-21042; Thermo Fisher; 1:1000). Doublets and dead cells were excluded based on forward and side scatters and DRAQ7 (Cat#7406S; Cell Signaling; 1:200) or DAPI fluorescence. hAEC2s were sorted as live/EpCAM+/HTII-280+ cells, and AHLM were sorted as live/CD45−/CD11b−/CD31−/EpCAM− cells.

Mouse lungs were incubated in the same digestion cocktail for 45 mins at 37 °C. The mixture was passed through a 70 μm cell strainer, resuspended in RBC lysis buffer, and filtered through a 40 μm cell strainer. Cells were stained with antibodies for 30 mins at 4 °C. Antibodies were used at 1:200: CD45-AF700 (Cat#560510; BD), CD31-APC/Fire750 (Cat#102528; BioLegend), and CD326-BV421 (Cat#563214; BD). mAEC2s were sorted using endogenous GFP from tamoxifen-induced $Sftpc^{creERT2/+}$:$R26R^{mTmG/+}$ lungs. AMLM were sorted based on the selection of live EpCAM−/CD45−/CD31−.

Freezing/Thawing primary human cells.

Cells were resuspended in F12 at 10^7 cells/mL, followed by addition of equal volume of 2x Freeze Solution (2% 1.5 M Hepes, 10% FBS, 78% F12, and 10% DMSO). Desired volume of cell aliquots was then frozen at −80 °C and stored in liquid nitrogen. Frozen cells were thawed and equal volume of warm recovery media (DMEM with 10% FBS) was added and incubated for 1 min, followed by addition of 12 mL of warm DMEM to the centrifuge tube. Cells were spun at 550 g for 4 mins and stained for FACS.

Cell culture

Mesenchymal cells were cultured in DMEM/F-12 (Cat#11330032; Thermo Fisher) with 10% FBS and 1% Pen/Strep. Cells were used within the first five passages of either receiving from ATCC (Cat#CCL-171) for MRC5 or isolating from donor lungs for AHLM. The construct pLKO5-tRFP (Addgene Plasmid #57823) was used to generate RFP-expressing lentiviruses (Lenti-RFP). For labelling AHLM, AHLM were transduced by Lenti-RFP with 10 μg/ml Polybrene (Cat#TR-1003-G, Millipore). iPSC-derived AEC2s with SFTPC−tdTomato reporter (iAEC2s)[23] were generated and maintained in CK+DCI media as described before[22]. Purity of iAEC2 culture was assessed at every passage by flow cytometry where a cell population with >96% tdTomato+ cells was considered pure as described before[22, 23].

Organoid assay

AEC2 and mesenchymal cells were co-cultured (5,000 AEC2 : 30,000 mesenchymal cells/well) in modified MTEC media diluted 1:1 in growth factor-reduced matrigel (Cat#CB-40230A; Thermo Fisher). Modified MTEC culture media is comprised of small airway basal media (SABM, Cat#CC-3118; Lonza) with Insulin, Transferrin, Bovine Pituitary Extract, Retinoic Acid, and EGF as per the SAGM Bullet Kit and 0.1 μg/mL cholera toxin (Cat#C8052; Sigma), 5% FBS, and 1% Pen/Strep. Cell suspension-matrigel mixture was placed in a transwell and incubated with 10 μM ROCK inhibitor (Cat#72252; STEMCELL) for the first 48 hrs. Each experimental condition was performed in triplicates. Where applicable, BMP4 (Cat#314-BP-010; R&D Systems; 50 ng/mL), TGFβ1 (Cat#100–21; Peprotech; 3 ng/mL), DMH-I (Cat#73632; STEMCELL; 1 μM), HHIP (Cat#9280-HP-050; R&D; 2.5 μg/mL), CHIR (Cat#4423; Tocris; 3 μM), and KGF (Cat#251KG01050; R&D; 100 ng/ml) were added to the media after 48 hrs and replenished in every media change. iAEC2s were co-cultured with either MRC5 or AHLM (5,000 AEC2s: 30,000 mesenchymal cells/well; both MRC5 and AHLM with passage<5) and maintained with either CK-DCI media or a 1:1 mixture of CK-DCI and modified MTEC media as described above. Colonies were assayed after 7, 14, and 21 days. For mesenchyme-free hAEC2 culture, hAEC2s were isolated from donor lungs via FACS as described above and cultured as previously described[21]. After two or three passages, purity of hAEC2s was assessed by protein staining for SFTPC and KRT5. Pure hAEC2s were then co-cultured with either MRC5 or AHLM as described above.

To extract RNA from organoids, cell-matrigel mixture in the transwell was washed with PBS and incubated in the lung digestion cocktail for 1 hr at 37°C with intermittent resuspension. The mixture was removed from the transwell and resuspended in TrypLE (Cat#12563011; Thermo Fisher) and shaken at 37°C for 20 mins. Cells were blocked with human FcR blocking reagent (Cat#564220; BD; 1:50) for 10 mins at 4°C, and then stained with biotin anti-CD326 (Cat#324216; BioLegend; 1:250) for 30 mins at 4°C. Streptavidin beads (Cat#17663; STEMCEL; 1:50) were added to isolate the epithelial cells, and the rest cells were mesenchymal cells. For sequencing, organoids were digested as above and FACS sorted for live EpCAM+ and EpCAM− cells.

qPCR

RNA was extracted from cells using PicoPure RNA Isolation Kit (Cat#KIT0204; Applied Biosystems). cDNA was synthesized from total RNA using SuperScript Strand Synthesis System (Cat#18080044, Thermo Fisher). qPCR was performed using SYBR Green (Cat#F415L; Thermo Fisher). Relative gene expression levels were defined using ΔΔCt method. qPCR primers (IDT) are listed in Supplementary Table 7.

RNA In Situ Hybridization

Paraformaldehyde-fixed OCT embedded sections were used for RNA in situ hybridization with RNAScope multiplex fluorescent v2 assay (ACDBio). Briefly, 7μm sections of normal or IPF lungs were washed, protease-dependent antigen retrieval was performed, and probes were hybridized for 2 hrs at 40°C, followed by step-wise amplification of each probe. RNA probes for *SFTPC* (Cat# 452561-C1, -C2; ACDBio), *KRT17* (Cat# 463661-C3; ACDBio),

and *CTHRC1* (Cat# 413331; ACDBio) were purchased and used. Following completion of RNA In Situ Hybridization, immunostaining was performed after blocking as stated earlier.

Xenotransplantation Assay

700,000 freshly sorted hAEC2s alone or mixed with 200,000 cultured AHLM or MRC5 cells (passage < 4) in 40 μL volume (1XPBS) were transplanted at 10 days post bleomycin injury into the lungs of NOD *scid* gamma mice via oral aspiration. Transplanted mice were euthanized 8–12 days post-transplant (a total of 18–22 days post bleomycin injury).

Single cell transcriptomics

Single cell sequencing was performed on a 10X Chromium instrument (10X Genomics) at the Institute of Human Genetics in UCSF as described before[37]. Briefly, cells were isolated via FACS and were then loaded on a Chromium Controller instrument to generate single-cell Gel Bead-In-EMulsions (GEMs). Libraries were prepared by performing reverse transcription on Bio-Rad C1000 Touch Thermal Cycler (Bio-Rad, Hercules, CA), following which, GEMs were harvested to amplify cDNA also using Bio-Rad C1000 Touch Thermal Cycler. SPRIselect (Beckman Coulter, Brea, CA) was used to select for amplified cDNA. Indexed sequencing libraries were constructed using the Chromium Single-Cell 3' library kit (10X Genomics) and sequenced on NovaSeq 6000 (Illumina) with the following parameters: Read 1 (26 cycles), Read 2 (98 cycles), and i7 index (8 cycles) to obtain a sequencing depth of ~100,000 read/cell. Reads were aligned to the appropriate mouse or human genome and quantified using the Cell Range Single-Cell Software Suite.

QUANTIFICATION AND STATISTICAL ANALYSIS

Statistical Analysis—All statistical analyses were performed in GraphPad Prism. Unpaired one-tailed t-tests were used to determine the p-value and data in graphs are presented as mean ± SD. For quantification of xenotransplants, Kolmogorov-Smirnov test was used to determine normality and one-way ANOVA followed by Kruskal-Wallis test was used for multiple comparisons. For normally distributed data, ordinary one-way ANOVA followed by Tukey's multiple comparisons test was performed. For all tests, p-values < 0.05 were considered significant. Representation factor calculated to represent the number of overlapping genes divided by the number of expected overlapping genes drawn from two independent groups, as calculated on nemates.org with a base value of 30,000 genes in human genome. A representation factor > 1 indicates more overlapping genes than expected of two independent groups.

Immunofluorescence Image Quantification—Sections were imaged for quantification on a Zeiss Lumar V12 or Zeiss AxioImager.M1 microscope. Cell counts for stained cells were performed on Fiji using the "Cell Counter" plug-in. Results were averaged between each specimen and SD were calculated per condition. For quantification of xenografts, at least three mice in each group were analyzed with at least two sections taken at 200 μm apart to capture different regions of the lung. Any HNA+ (human nuclear antigen) region of >5 cells was counted as one engrafted region. At least three lobes were analyzed at each section for three mice/condition; minimum of two sections/mouse were analyzed. Data are presented as mean ± SD. ** p < 0.01 (One way ANOVA followed by Kruskal-Wallis

for multiple comparison). For quantification of ABIs, at least six distinct areas per IPF specimen (n=3) covering at least three different zones of disease severity were counted. Zones of disease severity were defined as follows: 1) Normal looking alveoli - alveoli with a single layer of DAPI+ cells, 2) Thickened alveolar walls - alveoli with multiple layers of DAPI+ cells in the alveolar wall, 3) Microcysts - cyst-like structures that line and overlay the fibrotic regions as judged by accumulated DAPI+ cells in alveolar space, 4) Heavily fibrotic/bronchiolized zone - fibrotic lesions with autofluorescent collagen deposition around bronchiolized epithelium. *SFPTC*+/*KRT17*+/KRT5− cells were detected by mRNA in situ for *SFTPC* and *KRT17* and protein staining for KRT5 and were counted as ABI1s, *SFTPC*−/*KRT17*+/KRT5− cells were counted as ABI2s and *SFTPC*−/*KRT17*+/KRT5+ cells were counted as mature basal cells. IPF lung specimens (n=3) were probed with probes against *SFTPC*, *KRT17*, and *CTHRC1* mRNA and KRT5 protein staining to identify ABIs and adjacent CTHRC1+ mesenchyme. At least a 3×3 area was imaged at 20X (9 images), stitched together and counted as one data point. In total, 160 images were captured at 20X across three IPF lungs and every instance of ABI1, ABI2, or basal cell in actively remodeling region was counted. A cell cluster of at least 5 cells was counted as an ABI or a CTHRC1+ mesenchymal region. A mesenchymal region was marked as adjacent to ABIs if it was within 3 cell distance of an ABI cluster.

Analysis of single cell RNA-sequencing—FASTQ files were run through CellRanger v2.1.1 software with default settings for de-multiplexing, aligning reads with STAR software to Hg19 or GRCh38, and counting unique molecular identifiers (UMIs). Seurat packagev4.0[38] in R v3.5.1 was used for downstream analysis. Low quality cells were filtered (expressing less than 200 genes, > 10% mitochondrial reads and >6000 unique gene counts). Principal component analysis (PCA) was performed on log normalized and scaled data using 2000 variable genes. Top 10 PCAs were used for clustering, which were visualized using the Uniform Manifold Approximation and Projection (UMAP) algorithm in the Seurat package. Monocle trajectory analysis was performed using the Monocle 3[39] by importing the counts from the Seurat object. RNA velocity was calculated using scVelo v0.1.16 package[40] in Python v3.6 and velocity calculations were overlayed on UMAP projections calculated in Seurat. For single cell transcriptomes of healthy and IPF lungs were obtained from GSE135893 and GSE132771 and processed using Seurat. AEC2s, AEC1s, transitional AEC2s, KRT17+/KRT5− cells, and basal cells were extracted and analyzed. RNA values were averaged for each cluster using AverageExpression function followed by DoHeatmap function in Seurat to generate heatmaps. Genes specific to PATS-like cells reported in Kobayashi *et al.* were picked for heatmaps. The lists of differentially expressed genes were identified with a MAST test. Upstream regulator analysis of gene lists containing significantly differentially expressed genes (padj < 0.05, logFC < −0.15 or > 0.15) was done with Ingenuity Pathway Analysis (QIAGEN).

Bulk RNA Sequencing Analysis—Total RNA was extracted from AHLM and MRC5 cells using the RNeasy Kit (Cat#74004; QIAGEN). Sequencing was done using HiSeq 4000. Quality control of reads was conducted by using FastQC (Babraham Bioinformatics). Ligation adaptors were removed using the Cutadapt and Sickle 1.33. Sequencing reads were

aligned using STAR 2.7.9a and UCSC human GRCh38/hg38 was used as reference genome. The differential gene expression list was generated using DEseq2.

STATISTICS & REPRODUCIBILITY

No statistical method was used to predermine sample size. No data was excluded from analyses. Sample ID was blinded to investigator for image quantification.

DATA AVAILABILITY

The RNA-seq data that support the findings of this study have been deposited in the Gene Expression Omnibus (GEO) under the accession codes: GSE148992 (human bulkRNA-seq), GSE150068 (organoids and IPF), and GSE150247 (human scRNA-seq). Previously published scRNA-seq data that are re-analyzed here are available at GSE135893 and GSE132771. All other data supporting the findings of this study are available from the corresponding author on reasonable request.

CODE AVAILABILITY

No custom codes were developed and used in this manuscript. All codes are available by request to corresponding author.

Extended Data

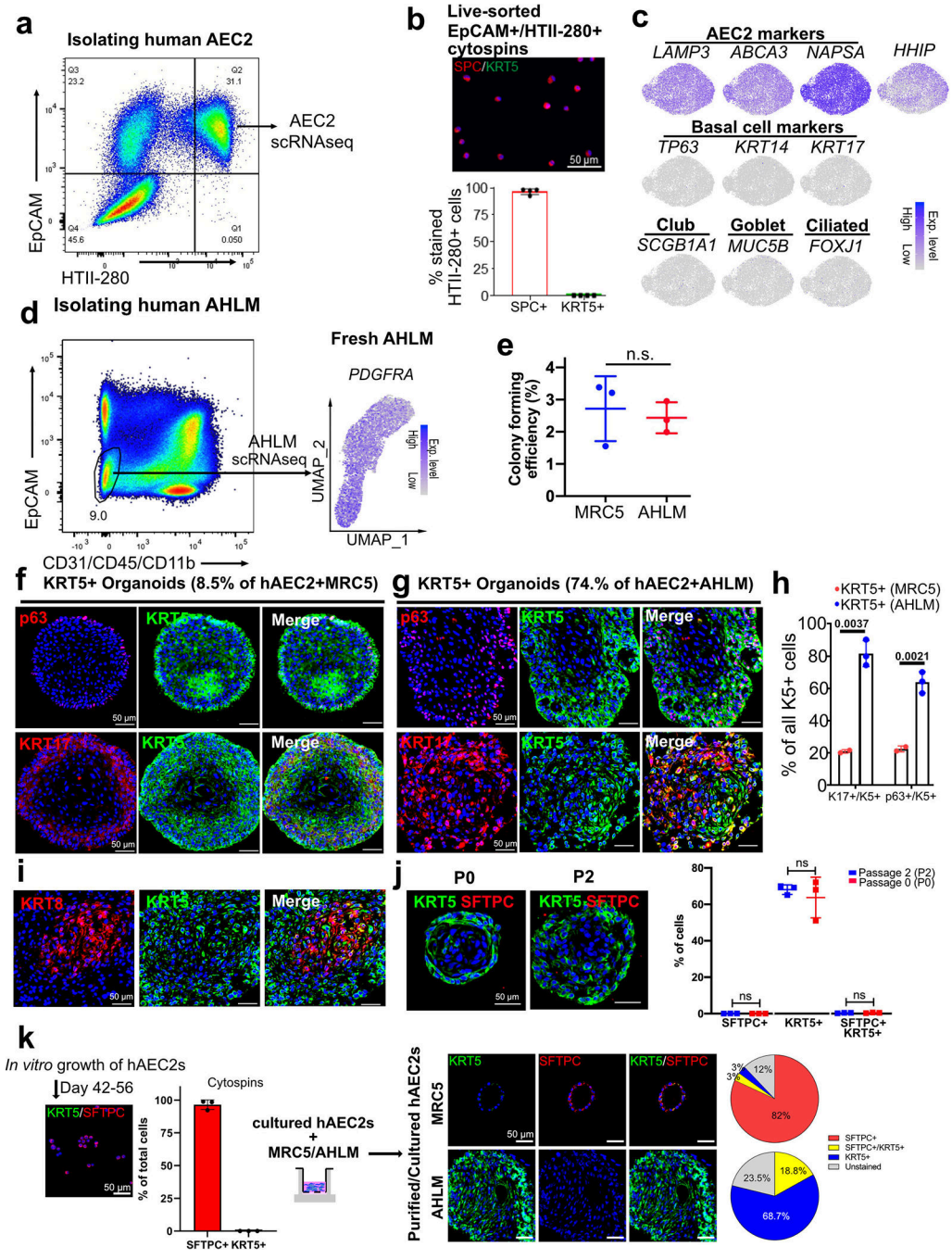

Extended Data Fig. 1: Purified hAEC2s transdifferentiate into KRT5+ basal cells when co-cultured with AHLM.

(**a**) FACS plot shows the strategy for isolating hAEC2s. After selecting live/CD45−/CD31−/CD11b− cells, hAEC2s were further isolated by gating EpCAM+/HTII-280+ cells. (**b**) Quantification of SFTPC+ and KRT5+ cells in freshly sorted HTII-280+ cells by cytospins. Data are mean ± SD, representative of n=4 biologically independent human lung cytospins analyzed. (**c**) confirmation of the purity of HTII-280+ cells by scRNAseq

showed no appreciable detection of non-AEC2 markers. (**d**) scRNA-seq of AHLM isolated as live/CD31−/CD45−/CD11b−/EpCAM− cells that express *PDGFRA*. (**e**) Colony forming efficiency of hAEC2/MRC5 and hAEC2/AHLM co-culture at D14. Data are mean ± SD, representative of n=3 biologically independent for AHLM and hAEC2 and representative of n=3 independent experiments for MRC5. (**f**) and (**g**) IF analysis of p63 and KRT17, and KRT5 in the hAEC2s+MRC5 and hAEC2s+AHLM organoids at D14. Images are representative of n=2 (in **f**) and n=3 (in **g**) biological replicates. (**h**) Quantification of KRT17+ and p63+ cells in total KRT5+ basal cells in the hAEC2s+MRC5 and hAEC2s+AHLM organoids at D14. n=2 (for MRC5) and n=3 (for AHLM) biologically independent samples were analyzed. Data are mean ± SD. (**i**) IF analysis of KRT8 in the hAEC2s+AHLM organoids at D14. Representative of n=2 independent experiments. (**j**) IF analysis and quantification of KRT5+ and SFTPC+ cells in the hAEC2-derived organoids co-cultured with freshly sorted AHLM (Passage 0) and cultured AHLM (Passage 2) at D14. Each dot represents a technical replicate. Representative of n=2 independent experiments. (**k**) Enrichment of hAEC2s using a mesenchyme-free system, confirmed by IF analysis and quantification of SFTPC+ and KRT5+ cells (left), and co-culture of the enriched hAEC2s with AHLM or MRC5, the organoids are analyzed at D14 (right). Data are expressed as the mean ± SD, representative of n=3 biologically independent experiments.

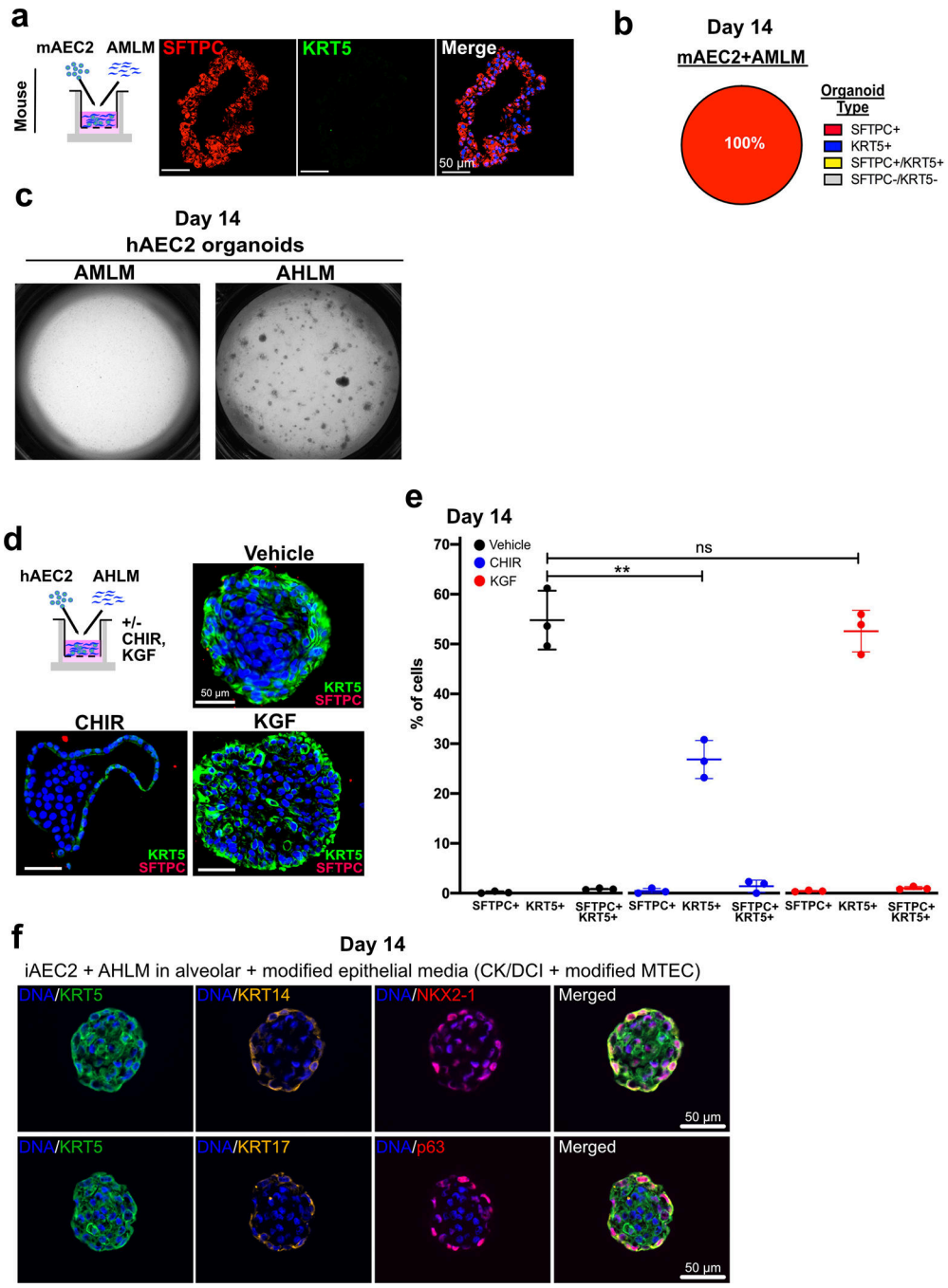

Extended Data Fig. 2: Difference in niche provided by mouse and human lung mesenchyme and components of the CK/DCI media on hAEC2s-to-basal transdifferentiation

(**a**) IF analysis of mouse AEC2s (mAEC2s)-derived organoids co-cultured with the adult mouse lung mesenchyme (AMLM) at D14. mAEC2s (GFP+) were sorted from the lung of adult *SftpcCreERT2/+:R26RmTmG/+* mouse. Representative of n=3 independent experiments. (**b**) Quantification of lineages of organoids (SFTPC+ organoids, organoids with both SFTPC+ cells and KRT5+ cells, or KRT5+ organoids) in mAEC2 + AMLM organoids. (**c**) hAEC2s co-cultured with either adult murine lung mesenchyme (AMLM)

or AHLM. (**d,e**) IF analysis and quantification of hAEC2 + AHLM organoids treated with 3 μM CHIR or 100 ng/ml KGF at D14. Representative of n=2 independent experiments. Data are expressed as the mean ± SD, representative of n=3 technical triplicates. ** p = 0.0012. (**f**) IF analysis of human iAEC2 + AHLM organoids cultured in 1:1 dilution of CK-DCI:SABM/MTEC standard media show canonical basal markers (KRT14, KRT17, P63) and lung lineage (NKX2–1). Data are expressed as the mean ± SD, representative of n=2 independent experiments. ** indicates $p < 0.01$ as determined by unpaired one-tailed student's t-test.

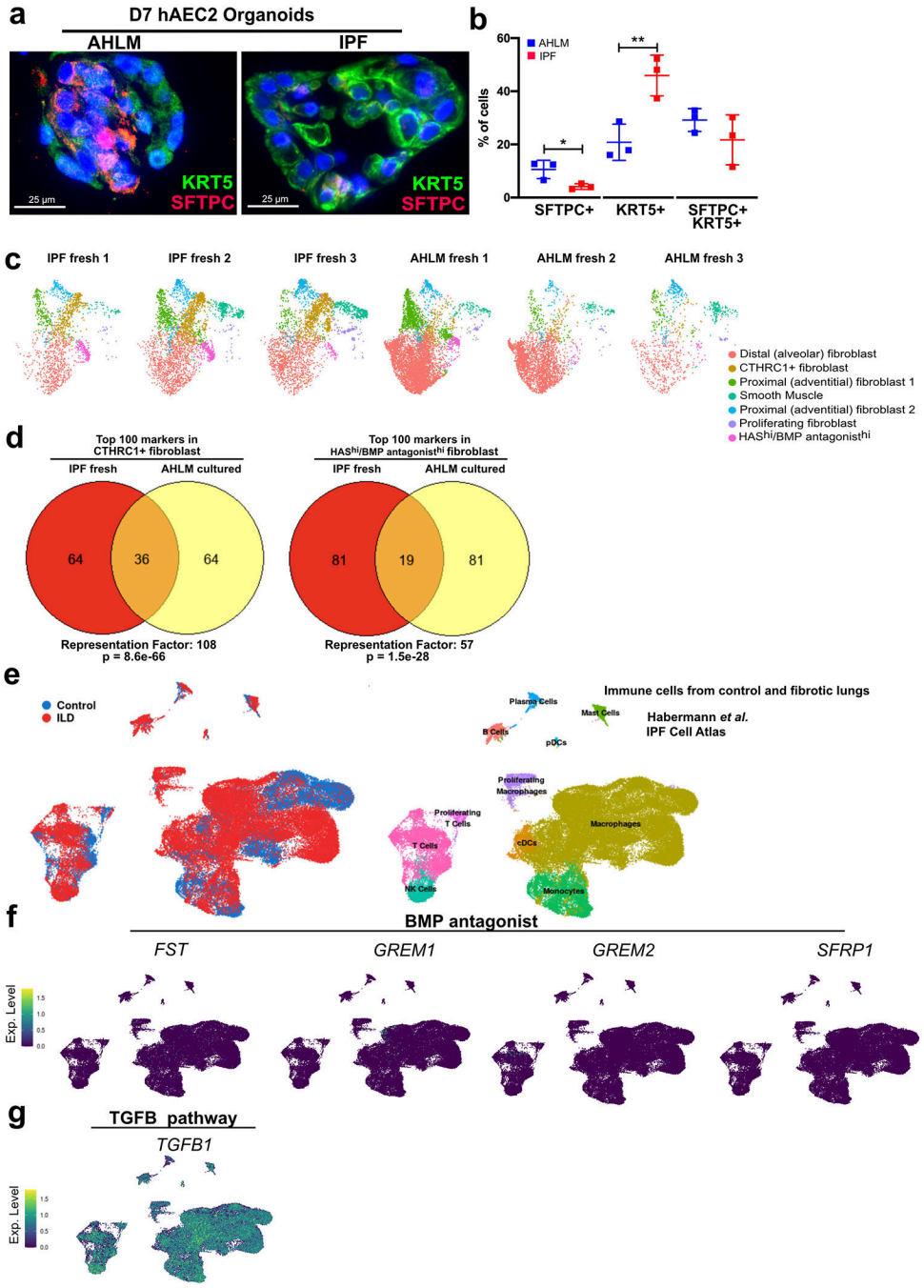

Extended Data Fig. 3: Comparison of pathologic mesenchymal niche subsets arising from IPF and cultured AHLM

(**a, b**) IF analysis of hAEC2s-derived organoids co-cultured with human adult normal lung (AHLM) and IPF mesenchyme at D7, and quantified by the percentage of SFTPC+, KRT5+, and SFTPC+/KRT5+ cells in total cells. Data are expressed as the mean ± SD, representative of n=3 technical replicates. * p = 0.0182 and ** p = 0.0066. Representative of n=2 independent experiments. (**c**) UMAP plots of mesenchyme from each individual IPF or normal donor that was used in scRNA-seq analysis. (**d**) Comparison of top 100 markers

in *CTHRC1*+ (left) and *HAS*^{high}/BMP anatgonist^{high} (right) clusters of uncultured IPF (IPF fresh) and cultured AHLM with statistical comparison for degree of gene overlap of two independent gene sets denoted by representation factor (see methods). (**e, f, and g**) UAMP plots show BMP antagonists and *TGFB1* expression in IPF lungs (from IPF Cell Atlas, Habermann et al.). Data are expressed as the mean ± SD. * indicates $p < 0.05$ and ** indicates $p < 0.01$ as determined by unpaired one-tailed student's t-test. Each data point on the graph represents a technical replicate.

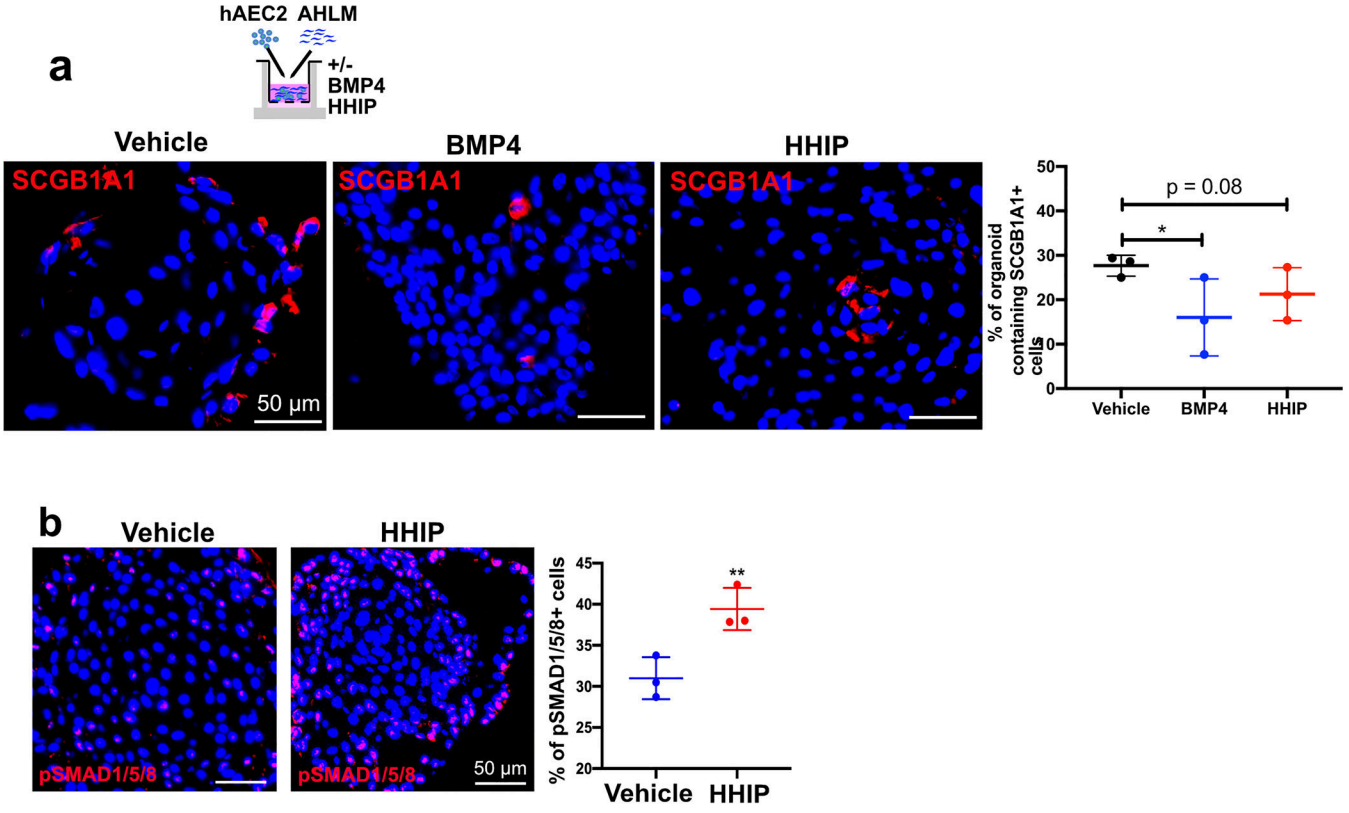

Extended Data Fig. 4: Effect of HHIP and BMP4 in modulating metaplastic hAEC2 transdifferentiation

(**a**) IF analysis of SCGB1A1 in the hAEC2+ AHLM organoids treated with 2.5 μg/ml HHIP and 50 ng/ml BMP4, quantified by percentage of organoid containing SCGB1A1+ cells. Data are expressed as the mean ± SD. * $p = 0.0441$. (**b**) IF analysis of pSMAD1/5/8 in the hAEC2+ AHLM organoids treated with 2.5 μg/ml HHIP, quantified by percentage of pSMAD1/5/8+ cells in total cells. Data are expressed as the mean ± SD. ** $p = 0.0079$. Experiment was performed in a technical triplicate. * indicates $p < 0.05$ and ** indicates $p < 0.01$ as determined by unpaired two-tailed student's t-test.

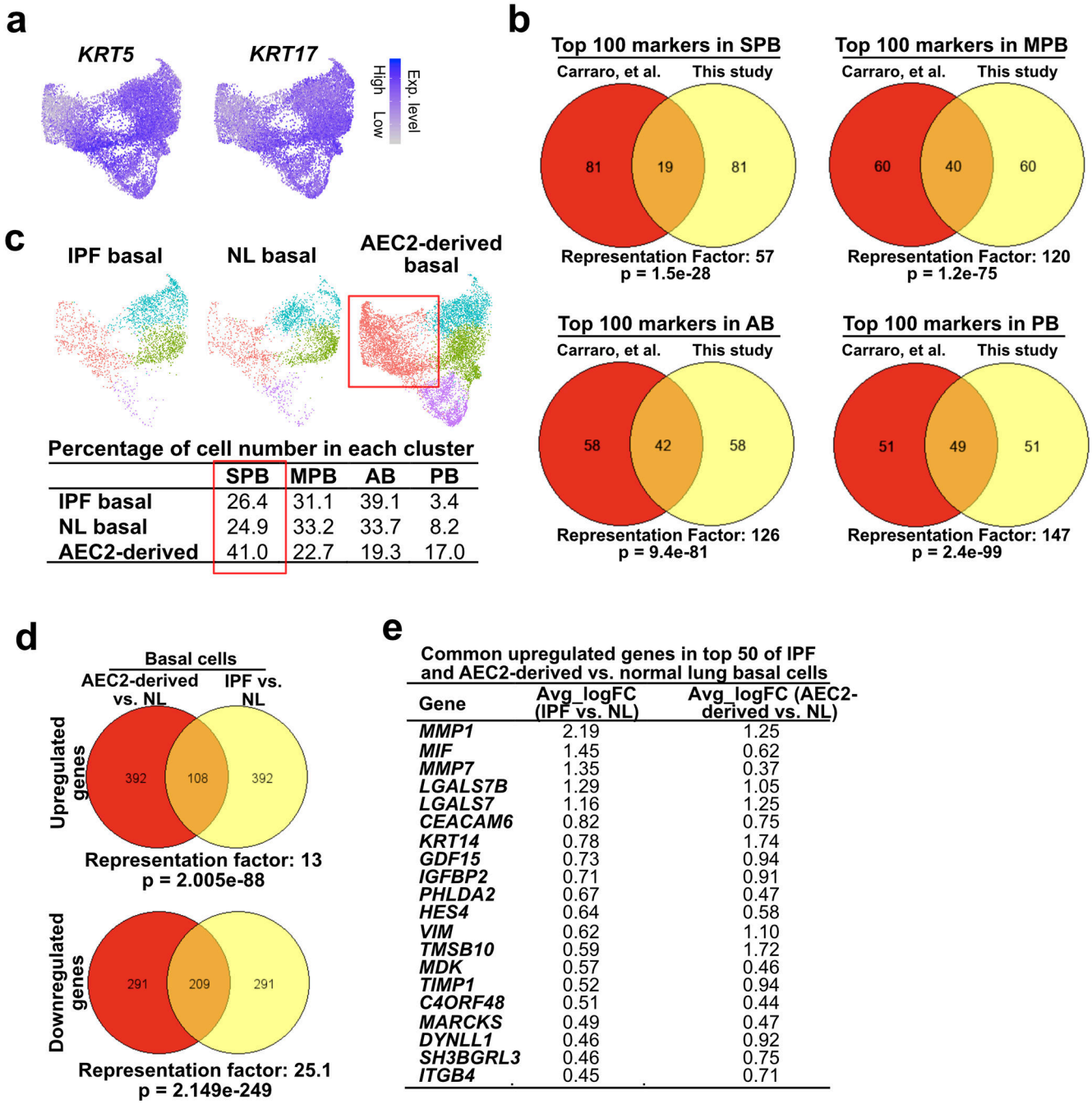

Extended Data Fig. 5: Comparison of hAEC2-derived and IPF basal cells

(**a**) Feature plots show KRT5 and KRT17 expression in the merged basal cell data from fresh normal donors (N = 2, marked as NL basal), fresh IPF patients (N = 2, marked as IPF basal), and hAEC2+AHLM organoids (N = 2). (**b**) Comparison of top 100 markers in SPB, MPB, AB, and PB clusters of this study and Carraro *et al.*[3] with statistical comparison for degree of gene overlap of two independent gene sets denoted by representation factor was done via http://nemates.org (see methods) (see methods). (**c**) UMAP plots of basal cells from IPF, normal donors, and hAEC2-derived organoids with contributing cell number in

each cluster. (**d**) Comparison of top 500 differentially expressed genes in hAEC2-derived and IPF basal cells against normal lung basal cells with statistical comparison for degree of gene overlap of two independent gene sets denoted by representation factor was done via http://nemates.org (see methods). (**e**) Representative upregulated genes in top 50 of IPF and hAEC2-derived vs. normal lung basal cells. SPB = secretory primed basal, MPB = multipotent basal, AB = activated basal, PB = proliferating basal.

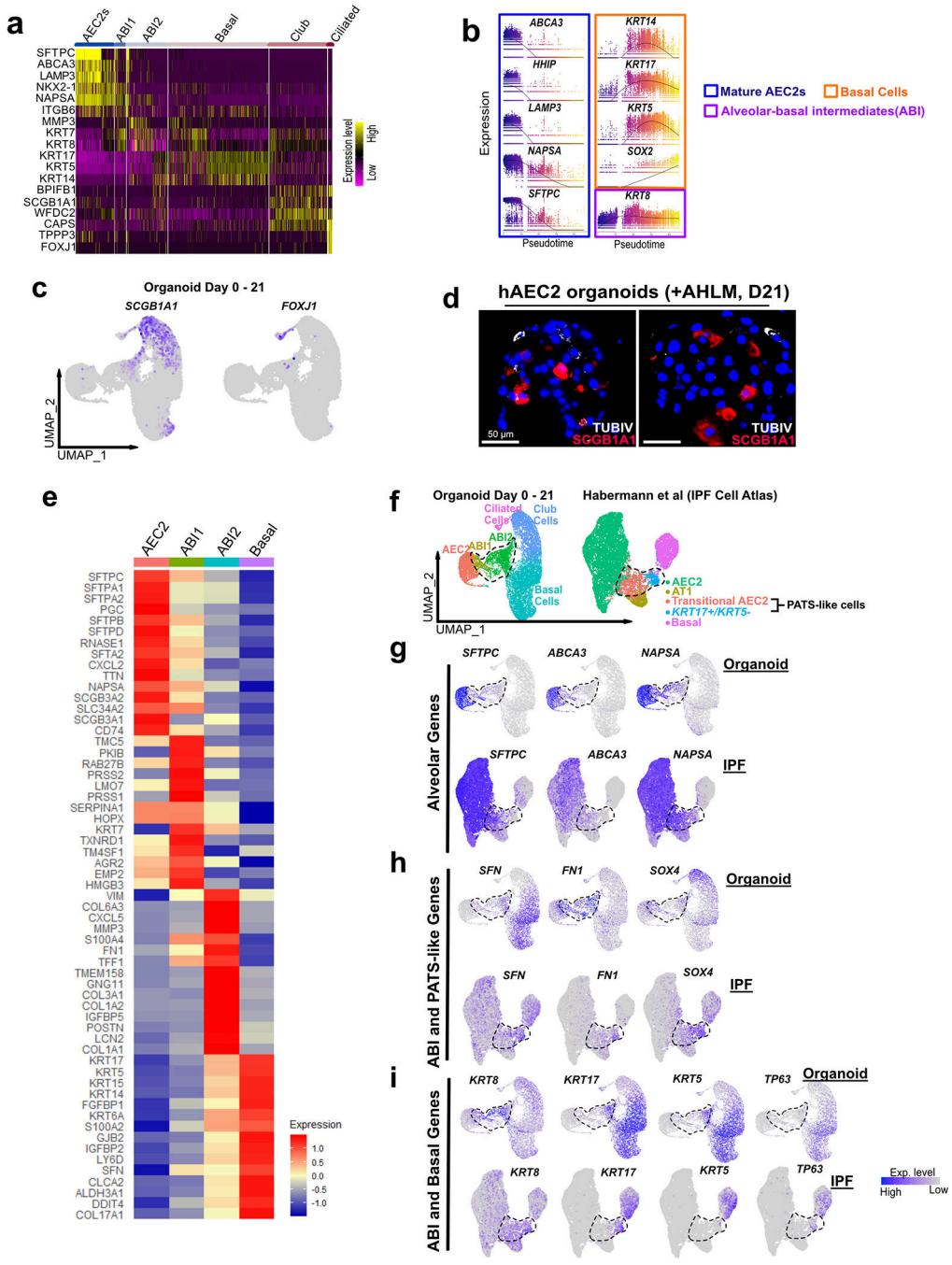

Extended Data Fig. 6: Expression of ABI markers in organoid and comparison with PATS-like cells in IPF.

(**a**) Heatmap of lineage marker expressions in different cellular subsets arising from hAEC2-derived organoids. (**b**) Expression along pseudotime trajectory of AEC2, ABI, and basal cell markers. (**c**) Featureplots of organoid scRNA-seq (D0-D21) show SCGB1A1+ club cells and FOXJ1+ ciliated cells. (**d**) IF staining of hAEC2+AHLM organoids (Day 21) show SCGB1A1+ club and rare TUBB4+ ciliated cells. Representative of n=2 independent experiments. (**e**) Top 15 significantly differentially expressed genes between AEC2s, ABI1s, ABI2s, and basal cells show AEC2-like profile of ABI1s and basal-like profile of ABI2s in addition to high ECM related gene signature of ABI2s. (**f**) UMAP of hAEC2-derived organoids cocultured with AHLM and IPF epithelium where transitional AEC2s and KRT17+/KRT5− cells as originally described by Habermann et al[4]. appear. The combination of transitional AEC2s and KRT17+/KRT5− cells were labeled as PATS-like cells by Kobayashi et al[1]. Feature plots comparing (**g**) hAEC2 lineage markers expression, (**h**) PATS-like markers expression, and (**i**) basal lineage marker expression in the UMAPs of organoid and IPF.

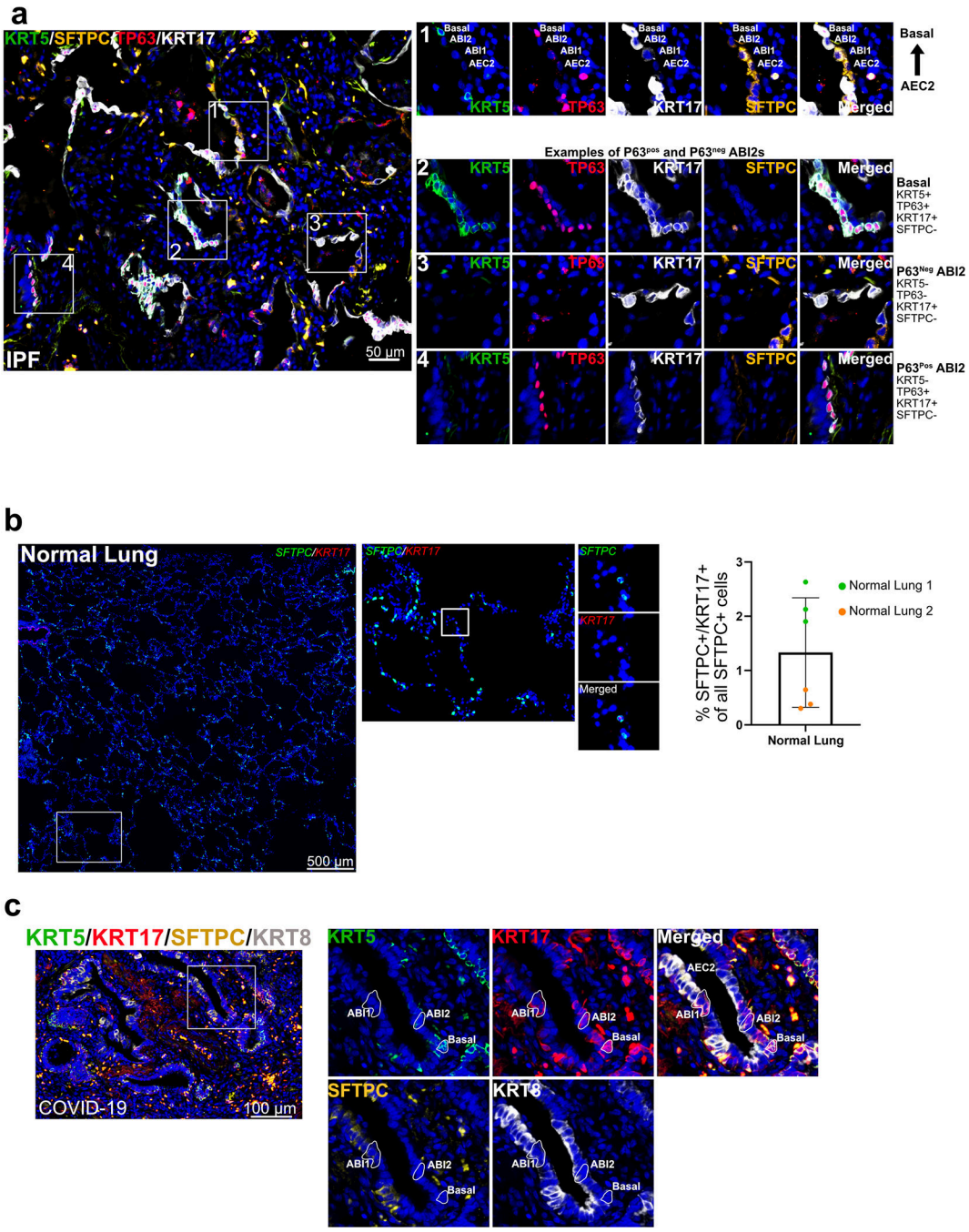

Extended Data Fig. 7: Identification of ABIs in normal, IPF, and COVID-19 lungs.

(**a**) Immunostaining of IPF lung with AEC2, ABIs, and basal markers show (**1**) linearly connected AEC2, ABI1, ABI2, and basal cell, (**2**) a cluster of basal cells (KRT17+/KRT5+/TP63+), and two types of ABI2s (KRT17+/KRT5−): (**3**) TP63^{neg} and (**4**) TP63^{pos}. Representative of n=3 independent IPF lungs. (**b**) In situ analysis hybridization of normal lung with *SFTPC* and *KRT17* identifies rare ABI1s (*SFTPC*+/*KRT17*+) as a fraction of total *SFTPC*+ cells. Data are represented as mean ± SD, representative of n=2 biologically independent samples. (**c**) Immunostaining of COVID-19 lung shows presence of AEC2s,

ABI1 and ABI2s, and basal cells in the same bronchiolized region. Representative of n=1 sample.

Supplementary Material

Refer to Web version on PubMed Central for supplementary material.

Acknowledgements

We thank Alisha Baldwin for providing technical assistance; Parnassus Flow Cytometry Core for assistance with cell sorting for bulk and single cell RNA analysis (P30DK063720); Eunice Wan and the Institute for Human Genetics Core for processing of single cell RNA samples and high-throughput sequencing. GEO accession number for raw RNA sequencing data is listed in Materials and Methods. This work is supported by NIH grants DP2AG056034, R01HL142552, and R01HL155622 to T.P., R01HL128484, R35HL150767 and U01HL134766 to H.C., F32HL143931–01A1 and K99HL155785–01 to J.J.K., Tobacco-related disease research program postdoctoral award to C.Q., and Nina Ireland Program Award to M.M. for human lung collection.

REFERENCES

1. Barkauskas CE et al. Type 2 alveolar cells are stem cells in adult lung. J Clin Invest 123, 3025–3036 (2013). [PubMed: 23921127]
2. Rock JR et al. Multiple stromal populations contribute to pulmonary fibrosis without evidence for epithelial to mesenchymal transition. Proc Natl Acad Sci U S A 108, E1475–1483 (2011). [PubMed: 22123957]
3. Smirnova NF et al. Detection and quantification of epithelial progenitor cell populations in human healthy and IPF lungs. Respir Res 17, 83 (2016). [PubMed: 27423691]
4. Xu Y et al. Single-cell RNA sequencing identifies diverse roles of epithelial cells in idiopathic pulmonary fibrosis. JCI Insight 1, e90558 (2016). [PubMed: 27942595]
5. Xi Y et al. Local lung hypoxia determines epithelial fate decisions during alveolar regeneration. Nat Cell Biol 19, 904–914 (2017). [PubMed: 28737769]
6. Vaughan AE et al. Lineage-negative progenitors mobilize to regenerate lung epithelium after major injury. Nature 517, 621–625 (2015). [PubMed: 25533958]
7. Liang J et al. Hyaluronan and TLR4 promote surfactant-protein-C-positive alveolar progenitor cell renewal and prevent severe pulmonary fibrosis in mice. Nat Med 22, 1285–1293 (2016). [PubMed: 27694932]
8. Habermann AC et al. Single-cell RNA sequencing reveals profibrotic roles of distinct epithelial and mesenchymal lineages in pulmonary fibrosis. Sci Adv 6, eaba1972 (2020). [PubMed: 32832598]
9. Adams TS et al. Single-cell RNA-seq reveals ectopic and aberrant lung-resident cell populations in idiopathic pulmonary fibrosis. Sci Adv 6, eaba1983 (2020). [PubMed: 32832599]
10. Kumar PA et al. Distal airway stem cells yield alveoli in vitro and during lung regeneration following H1N1 influenza infection. Cell 147, 525–538 (2011). [PubMed: 22036562]
11. Ray S et al. Rare SOX2(+) Airway Progenitor Cells Generate KRT5(+) Cells that Repopulate Damaged Alveolar Parenchyma following Influenza Virus Infection. Stem Cell Reports 7, 817–825 (2016). [PubMed: 27773701]
12. Yang Y et al. Spatial-Temporal Lineage Restrictions of Embryonic p63(+) Progenitors Establish Distinct Stem Cell Pools in Adult Airways. Dev Cell 44, 752–761 e754 (2018). [PubMed: 29587145]
13. Pan H, Deutsch GH, Wert SE, Ontology S & Consortium NMAo.L.D.P. Comprehensive anatomic ontologies for lung development: A comparison of alveolar formation and maturation within mouse and human lung. J Biomed Semantics 10, 18 (2019). [PubMed: 31651362]
14. Prasse A et al. BAL Cell Gene Expression Is Indicative of Outcome and Airway Basal Cell Involvement in Idiopathic Pulmonary Fibrosis. Am J Respir Crit Care Med 199, 622–630 (2019). [PubMed: 30141961]

15. Zacharias WJ et al. Regeneration of the lung alveolus by an evolutionarily conserved epithelial progenitor. Nature 555, 251–255 (2018). [PubMed: 29489752]
16. Wang C et al. Expansion of hedgehog disrupts mesenchymal identity and induces emphysema phenotype. J Clin Invest 128, 4343–4358 (2018). [PubMed: 29999500]
17. Jiang P et al. Ineffectual AEC2-to-AEC1 Differentiation in IPF: Persistence of KRT8(hi) Transitional State. Am J Respir Crit Care Med (2020).
18. Choi J et al. Inflammatory Signals Induce AT2 Cell-Derived Damage-Associated Transient Progenitors that Mediate Alveolar Regeneration. Cell Stem Cell 27, 366–382 e367 (2020). [PubMed: 32750316]
19. Strunz M et al. Alveolar regeneration through a Krt8+ transitional stem cell state that persists in human lung fibrosis. Nat Commun 11, 3559 (2020). [PubMed: 32678092]
20. Kobayashi Y et al. Persistence of a regeneration-associated, transitional alveolar epithelial cell state in pulmonary fibrosis. Nat Cell Biol 22, 934–946 (2020). [PubMed: 32661339]
21. Katsura H et al. Human Lung Stem Cell-Based Alveolospheres Provide Insights into SARS-CoV-2-Mediated Interferon Responses and Pneumocyte Dysfunction. Cell Stem Cell 27, 890–904 e898 (2020). [PubMed: 33128895]
22. Jacob A et al. Differentiation of Human Pluripotent Stem Cells into Functional Lung Alveolar Epithelial Cells. Cell Stem Cell 21, 472–488 e410 (2017). [PubMed: 28965766]
23. Hurley K et al. Reconstructed Single-Cell Fate Trajectories Define Lineage Plasticity Windows during Differentiation of Human PSC-Derived Distal Lung Progenitors. Cell Stem Cell 26, 593–608 e598 (2020). [PubMed: 32004478]
24. Weiner AI et al. Mesenchyme-free expansion and transplantation of adult alveolar progenitor cells: steps toward cell-based regenerative therapies. NPJ Regen Med 4, 17 (2019). [PubMed: 31452939]
25. Tsukui T et al. Collagen-producing lung cell atlas identifies multiple subsets with distinct localization and relevance to fibrosis. Nat Commun 11, 1920 (2020). [PubMed: 32317643]
26. Cassandras M et al. Gli1(+) mesenchymal stromal cells form a pathological niche to promote airway progenitor metaplasia in the fibrotic lung. Nat Cell Biol 22, 1295–1306 (2020). [PubMed: 33046884]
27. Travaglini KJ et al. A molecular cell atlas of the human lung from single-cell RNA sequencing. Nature 587, 619–625 (2020). [PubMed: 33208946]
28. Carraro G et al. Single-Cell Reconstruction of Human Basal Cell Diversity in Normal and Idiopathic Pulmonary Fibrosis Lungs. Am J Respir Crit Care Med 202, 1540–1550 (2020). [PubMed: 32692579]
29. Rosas IO et al. MMP1 and MMP7 as potential peripheral blood biomarkers in idiopathic pulmonary fibrosis. PLoS Med 5, e93 (2008). [PubMed: 18447576]
30. Ning J, Zhao Y, Ye Y & Yu J Opposing roles and potential antagonistic mechanism between TGF-beta and BMP pathways: Implications for cancer progression. EBioMedicine 41, 702–710 (2019). [PubMed: 30808576]
31. Dituri F, Cossu C, Mancarella S & Giannelli G The Interactivity between TGFbeta and BMP Signaling in Organogenesis, Fibrosis, and Cancer. Cells 8 (2019).
32. Basil MC et al. The Cellular and Physiological Basis for Lung Repair and Regeneration: Past, Present, and Future. Cell Stem Cell 26, 482–502 (2020). [PubMed: 32243808]
33. Chapman HA et al. Integrin alpha6beta4 identifies an adult distal lung epithelial population with regenerative potential in mice. J Clin Invest 121, 2855–2862 (2011). [PubMed: 21701069]
34. Muzumdar MD, Tasic B, Miyamichi K, Li L & Luo L A global double-fluorescent Cre reporter mouse. Genesis 45, 593–605 (2007). [PubMed: 17868096]
35. Coughlan AM et al. Myeloid Engraftment in Humanized Mice: Impact of Granulocyte-Colony Stimulating Factor Treatment and Transgenic Mouse Strain. Stem Cells Dev 25, 530–541 (2016). [PubMed: 26879149]
36. Shultz LD et al. Human lymphoid and myeloid cell development in NOD/LtSz-scid IL2R gamma null mice engrafted with mobilized human hemopoietic stem cells. J Immunol 174, 6477–6489 (2005). [PubMed: 15879151]

37. Kathiriya JJ, Brumwell AN, Jackson JR, Tang X & Chapman HA Distinct Airway Epithelial Stem Cells Hide among Club Cells but Mobilize to Promote Alveolar Regeneration. Cell Stem Cell 26, 346–358 e344 (2020). [PubMed: 31978363]

38. Stuart T et al. Comprehensive Integration of Single-Cell Data. Cell 177, 1888–1902 e1821 (2019). [PubMed: 31178118]

39. Cao J et al. The single-cell transcriptional landscape of mammalian organogenesis. Nature 566, 496–502 (2019). [PubMed: 30787437]

40. Bergen V, Lange M, Peidli S, Wolf FA & Theis FJ Generalizing RNA velocity to transient cell states through dynamical modeling. Nat Biotechnol 38, 1408–1414 (2020). [PubMed: 32747759]

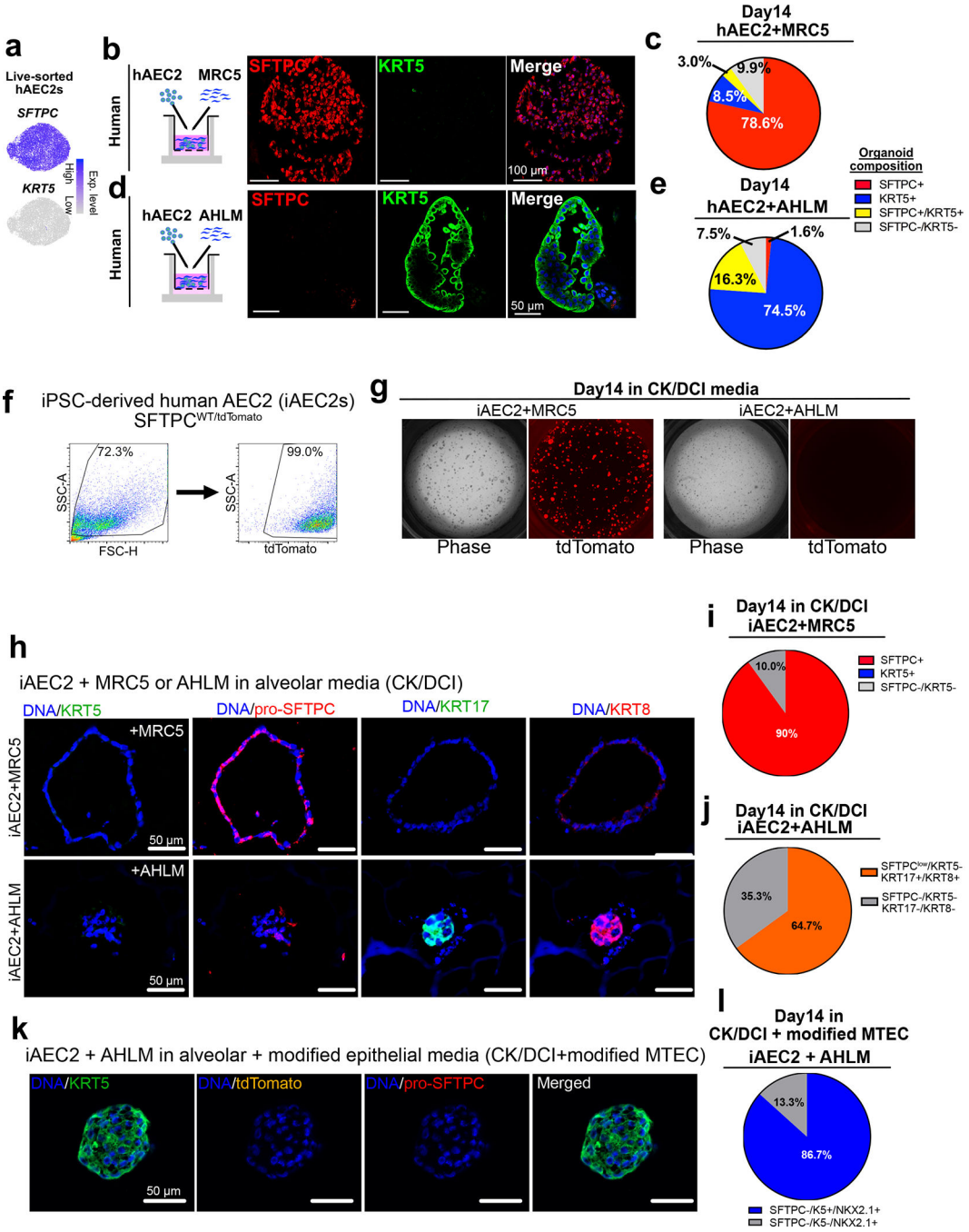

Figure 1. Primary adult human lung mesenchyme (AHLM) drives human AEC2 (hAEC2) transdifferentiation into KRT5+ basal cells *in vitro*.

(**a**) Live/EpCAM+/HTII-280+ cells (hAEC2s) were sorted and sequenced, confirming purified *SFTPC+* population. (**b,c**) IF of hAEC2-derived organoids co-cultured with MRC5 with quantification of epithelial lineages found in the organoids (SFTPC+ organoids, organoids with both SFTPC+ cells and KRT5+ cells, or KRT5+ organoids). representative of n=3 biologically independent replicates. Data are presented as mean of the two replicates. (**d,e**) IF of hAEC2-derived organoids co-cultured with AHLM with quantification of

lineages of organoids. Data are presented as mean of n=2 biological samples. Representative of n=2 independent experiments. (**f**) iPSC-derived AEC2s express tdTomato from one allele of *SFTPC* and can be flow purified based on their tdTomato expression. (**g**) iAEC2s were co-cultured with either MRC5 or AHLM (both passage < 5) with CK+DCI media and organoids were analyzed at D14 for tdTomato expression. Experiments were performed in biological duplicates with AHLM harvested from two independent donor lungs. (**h**) Organoids from iAEC2s/MRC5 or iAEC2s/AHLM were harvested and stained for alveolar (SFTPC), basal (KRT5 or KRT17), or intermediate (KRT8) markers. (**i**) 90% of iAEC2s/MRC5 organoids were SFTPC+/tdTomato+, while (**j**) ~65% of iAEC2s/AHLM organoids were $SFTPC^{low}$, with the rest $SFTPC^{neg}$. These organoids were also KRT5−/KRT17+/KRT8+, suggesting only partial differentiation. Representative of n=2 independent experiments. (**k, l**) iAEC2/AHLM organoids, when co-cultured with 1:1 mixture of CK-DCI and modified MTEC media show complete transdifferentiation of tdTomato+ iAEC2s into tdTomato−/SFTPC−/KRT5+/NKX2–1+ (86.7% of analyzed colonies) lung basal cells. The remaining 13.3% of organoids were SFTPC−/K5−/NKX2–1+. Representative of n=2 independent experiments.

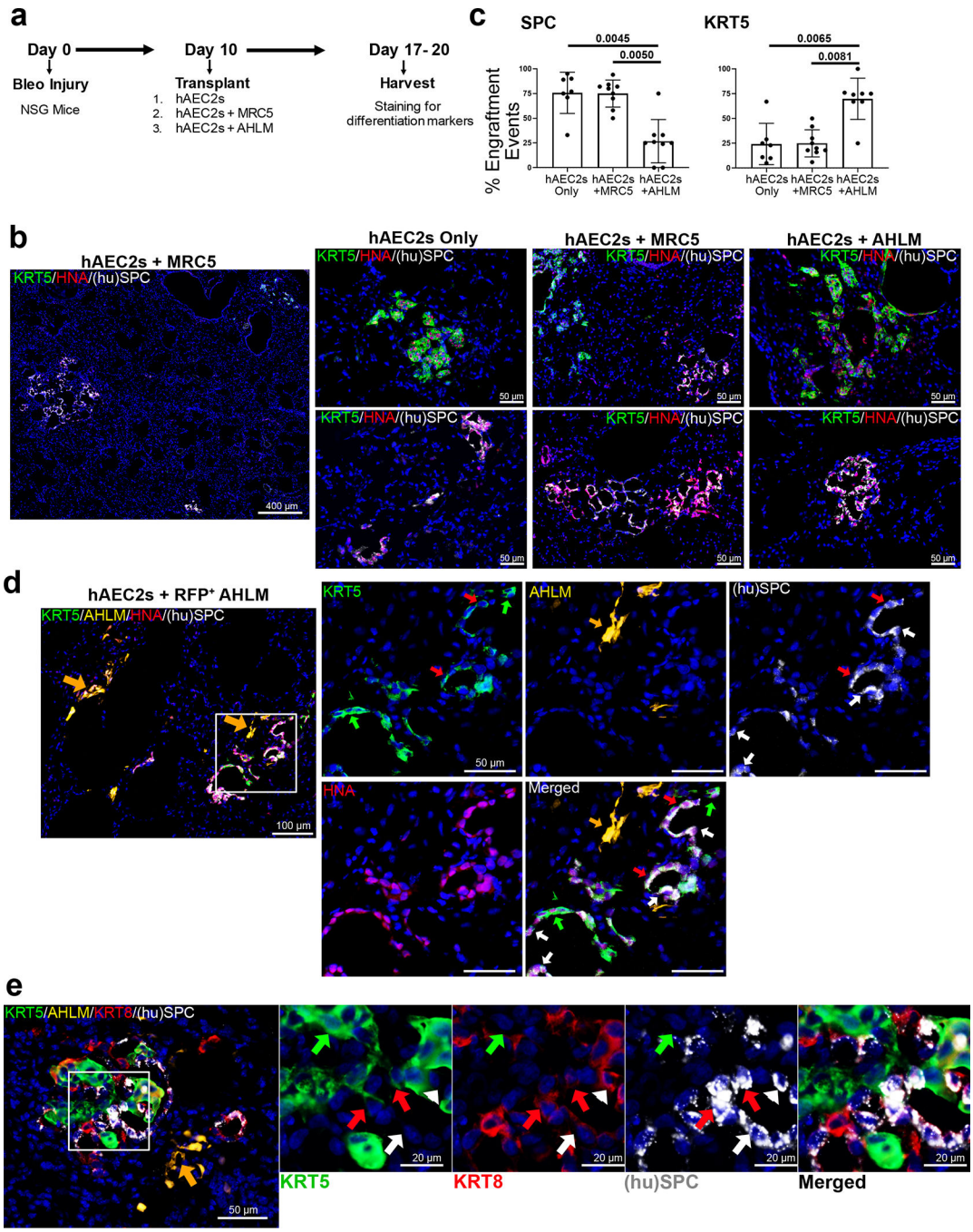

Figure 2. hAEC2 is capable of metaplastic KRT5+ transdifferentiation in a fibrotic host *in vivo*.

(**a**) Experimental setup of xenotransplant experiment testing engraftment of hAEC2s alone or co-transplanted with MRC5 or AHLM. (**b**) hAEC2s engrafted in the injured lungs and differentiated towards either KRT5+ (green) basal cells or remained as pro-SFTPC+ (white) hAEC2s as judged by co-staining with human nuclear antigen (HNA, red) in the lungs of mice transplanted with hAEC2s alone or hAEC2s+MRC5 or hAEC2s+AHLM. n=3 mice/group, representative of n=2 independent replicates. (**c**) Co-transplantation of hAEC2s with MRC5 cells does not change relative rates of hAEC2s engraftment events when compared

with hAEC2s alone. However, co-transplantation of AHLM reduced the number of hAEC2 patches observed in the lungs of mice while increasing basal cell differentiation. Each dot represents the number of engrafted regions (> 5 cells) in one section. At least two sections/mouse were analyzed and n=3 mice/group. Data are expressed as the mean ± SD. Kolmogorov-Smirnov test was used to determine normality and one-way ANOVA followed by Kruskal-Wallis test was used for multiple comparisons. (**d**) IF of engrafted hAEC2s actively transdifferentiating into KRT5+ basal cells in proximity to engrafted AHLM in the injured lung. Orange arrows: RFP-labeled AHLM, green arrows: KRT5+/SFTPC− basal cells, white arrows: SFTPC+/KRT5− hAEC2s, red arrows: KRT5+/SFTPC+ hybrid cells. n=3 mice/group, representative of one independent experiment. (**e**) Immunostaining of lungs transplanted with hAEC2 and tdTomato−labeled AHLM showed $KRT8^{low}$/SFTPC+ hAEC2s (white arrows; inset), KRT8+/SFTPC+ intermediate-hAEC2s (white arrowhead; inset), KRT5+ basal cells (green arrows; inset), and rare SFTPC+/KRT5+ cells (red arrows; inset) adjacent to tdTomato−labeled AHLM (orange arrow) in areas of engraftment. Data are representative of n=3 mice.

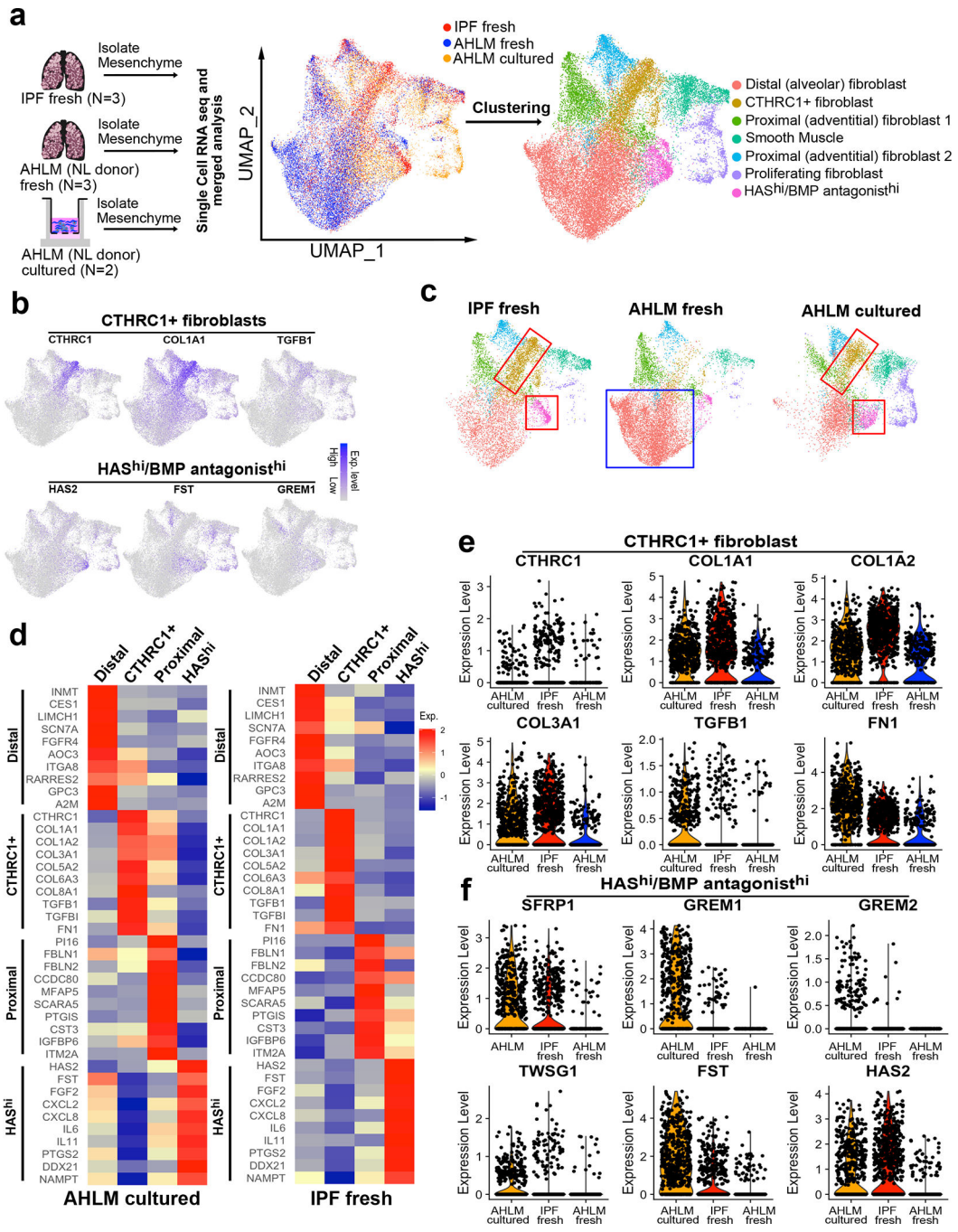

Figure 3. Emergence of pathologic mesenchymal niche subsets previously seen in IPF from cultured AHLM

(**a**) scRNAseq analysis of fresh (sorted from donor lung, uncultured) AHLM (normal donors, N = 3, marked as AHLM fresh), fresh IPF mesenchyme (N = 3, marked as IPF fresh), and cultured AHLM at passage 0–1 isolated from organoids (N = 2). (**b**) Signature genes in *CTHRC1*+ and *HAS*^{hi}/BMP antagonist^{hi} clusters. (**c**) scRNAseq analysis showing decrease of distal (alveolar) population (blue box) and increase of *CTHRC1*+ and *HAS*^{hi}/BMP antagonist^{hi} populations (red boxes) in both fresh IPF mesenchyme

and cultured AHLM. (**d**) Heat maps show the signature genes of each cluster in fresh IPF mesenchyme and cultured AHLM. (**e**) Violin plots show the signature genes in the *CTHRC1*+ fibroblasts among AHLM cultured, IPF fresh, and AHLM fresh. (**f**) Violin plots show the BMP antagonists in the HAS^{hi}/BMP $antagonist^{hi}$ fibroblasts among AHLM cultured, IPF fresh, and AHLM fresh.

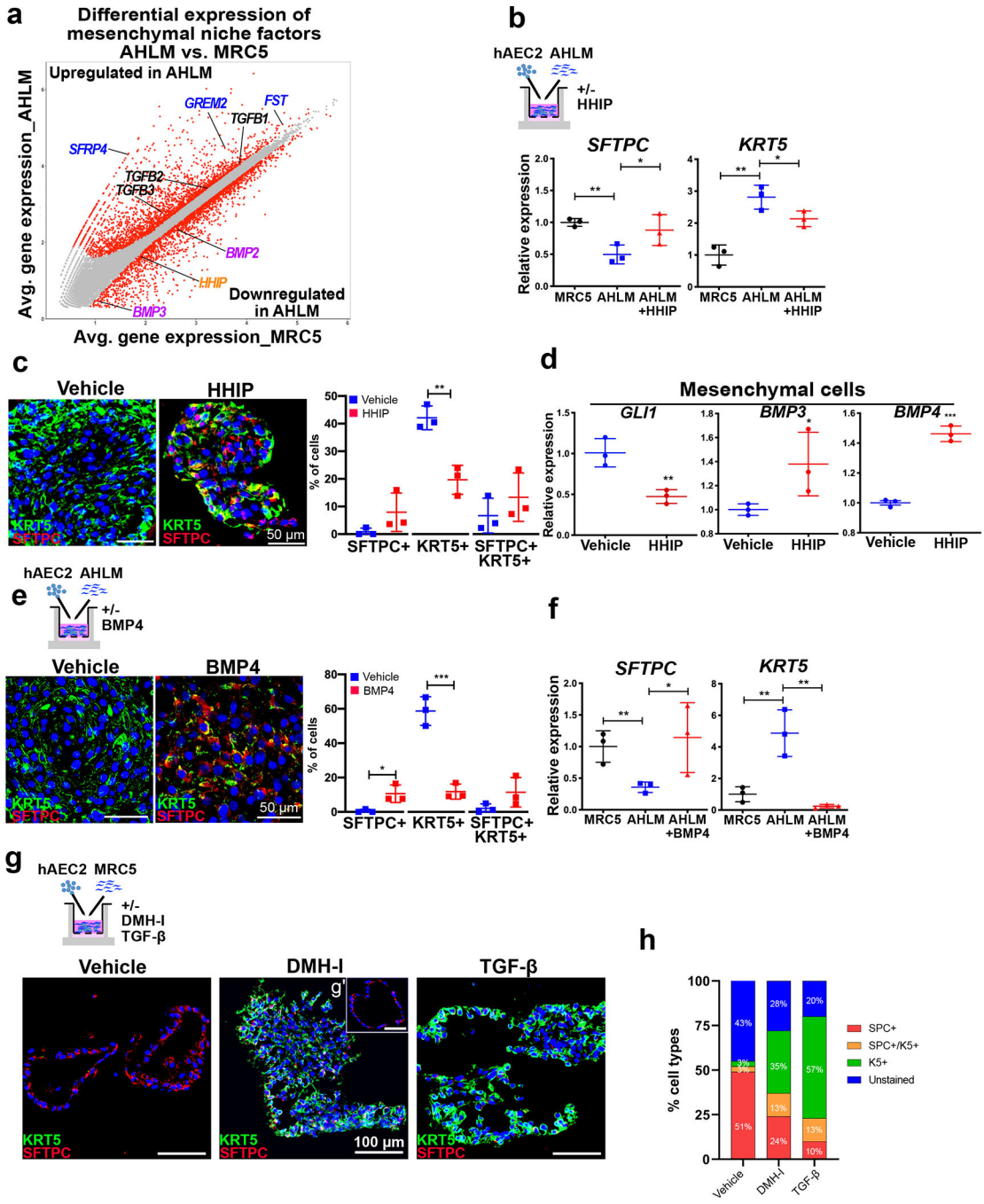

Figure 4. hAEC2-intrinsic and niche factors altered in IPF modulate metaplastic hAEC2 transdifferentiation.

(**a**) Bulk RNA-seq analysis of AHLM and MRC5 with differential gene expression analysis. Significantly differentially expressed genes (padj < 0.01, log2FC < −0.5 or > 0.5) were marked as red dots, otherwise in grey. (**b**) Treatment of hAEC2s+AHLM organoids with 2.5 μg/ml HHIP increases *SFTPC* and decreases *KRT5* expression in the epithelial fractions at D14 of co-culture. The expression levels of SFTPC and KRT5 in the epithelial fractions of hAEC2s+MRC5 organoids were used as controls. Data are expressed as the mean ±

SD. *SFTPC*: ** p = 0.0028 and * p = 0.0399; *KRT5*: ** p = 0.0015 and * p = 0.0294. (**c**) IF analysis of HHIP-treated hAEC2s+AHLM organoids at D14, and quantified by the percentage of SFTPC+, KRT5+, and SFTPC+/KRT5+ cells in total cells. Data are expressed as the mean ± SD. ** p = 0.0023. (**d**) HHIP-treated AHLM isolated from D14 organoid co-culture demonstrates decreased *GLI1* and increased *BMP3* and *BMP4* mRNA levels. Data are expressed as the mean ± SD. ** p = 0.0043, * p = 0.0354, and *** p = 0.0002. (**e**) IF analysis and quantification of the hAEC2s+AHLM organoids at D14 treated with 50 ng/ml BMP4. Data are expressed as the mean ± SD. * p = 0.0142 and *** p = 0.0005. (**f**) Treatment of hAEC2s+AHLM organoids with BMP4 increases *SFTPC* and decreases *KRT5* mRNA expression in the epithelial fractions at D14 of co-culture. The expression levels of *SFTPC* and *KRT5* in the epithelial fractions of hAEC2s+MRC5 organoids were used as controls. Data are expressed as the mean ± SD. *SFTPC*: ** p = 0.0066 and * p = 0.0358; *KRT5*: ** p = 0.0062 and ** p = 0.0028. (**g,h**) IF analysis of D14 hAEC2s+AHLM organoids treated with DMH-I (1 μM) or TGFβ1 (3 ng/mL). DMH-I treatment gives rise to either SFTPC+ alveolospheres (**g'**, 24% SFTPC+ AEC2s) or KRT5+/SFTPC+ basal/AEC2 mixed colonies (35% KRT5+ basal cells). TGFβ1 treatment drives more efficient basal cell transdifferentiation by suppressing alveolar fate (10% SFTPC+ AEC2s) and induces basal fate (57% KRT5+ basal cells). Experiment was performed in a technical triplicate and data from three technical replicates are counted as one biological replicate. * indicates $p < 0.05$ and ** indicates $p < 0.01$ as determined by unpaired two-tailed student's t-test. Each data point on graph represents one technical replicate.

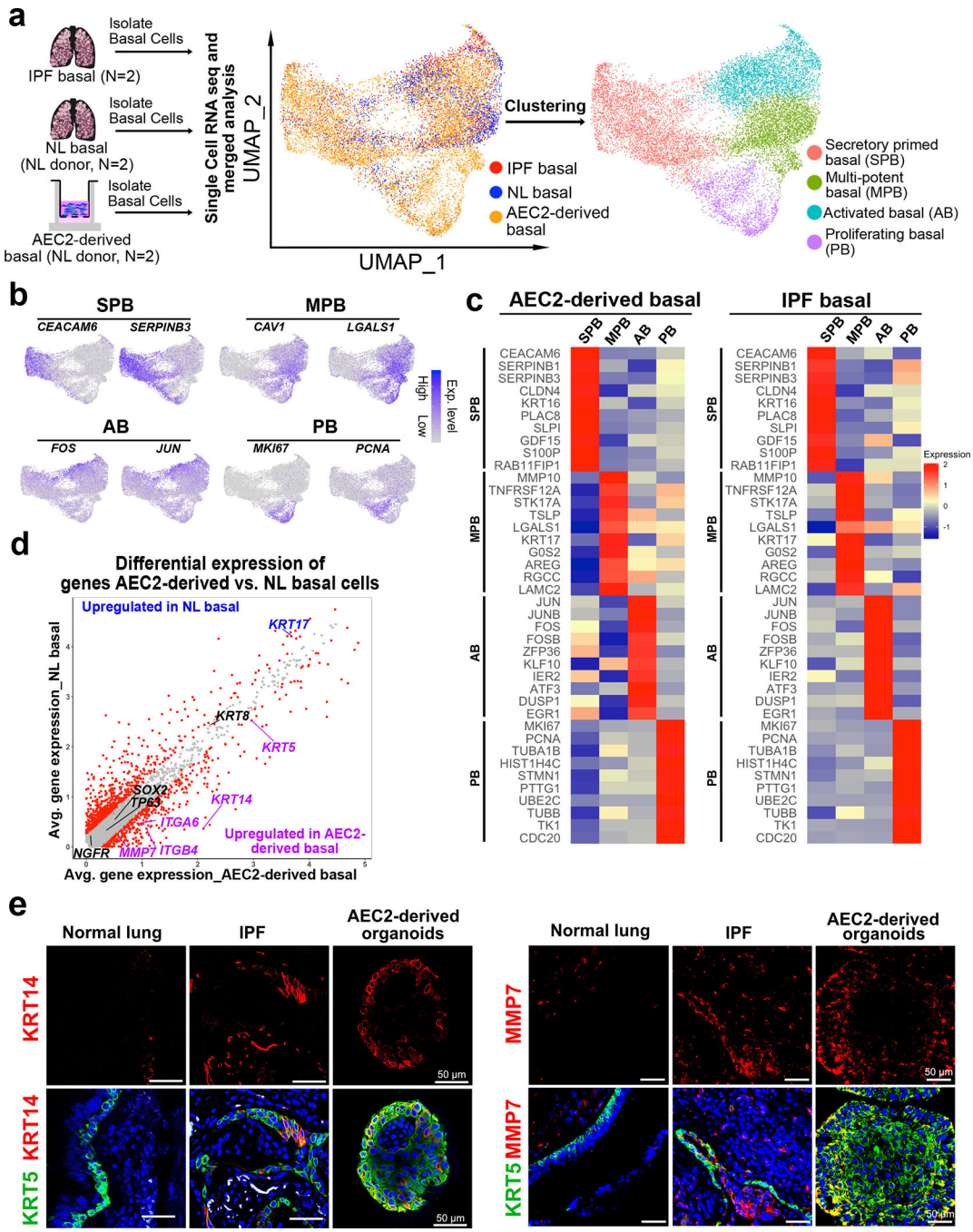

Figure 5. hAEC2-derived basal cells resemble metaplastic basal cells seen in IPF

(**a**) scRNAseq analysis of basal cells from fresh normal donors (N = 2, marked as NL basal), fresh IPF patients (N = 2, marked as IPF basal), and hAEC2+AHLM organoids (N = 2). (**b**) Signature genes in SPB, MPB, AB, and PB clusters. (**c**) Heat maps show the signature genes of each cluster in hAEC2-derived basal and IPF basal cells. (**d**) Differential gene expression analysis of hAEC2-derived basal vs. IPF basal cells. (**e**) IF analysis of KRT14, MMP7, and KRT5 in normal lung, IPF lung, and hAEC2-derived organoids at D14. Representative of

n=2 independent experiments. SPB = secretory primed basal, MPB = multipotent basal, AB = activated basal, PB = proliferating basal.

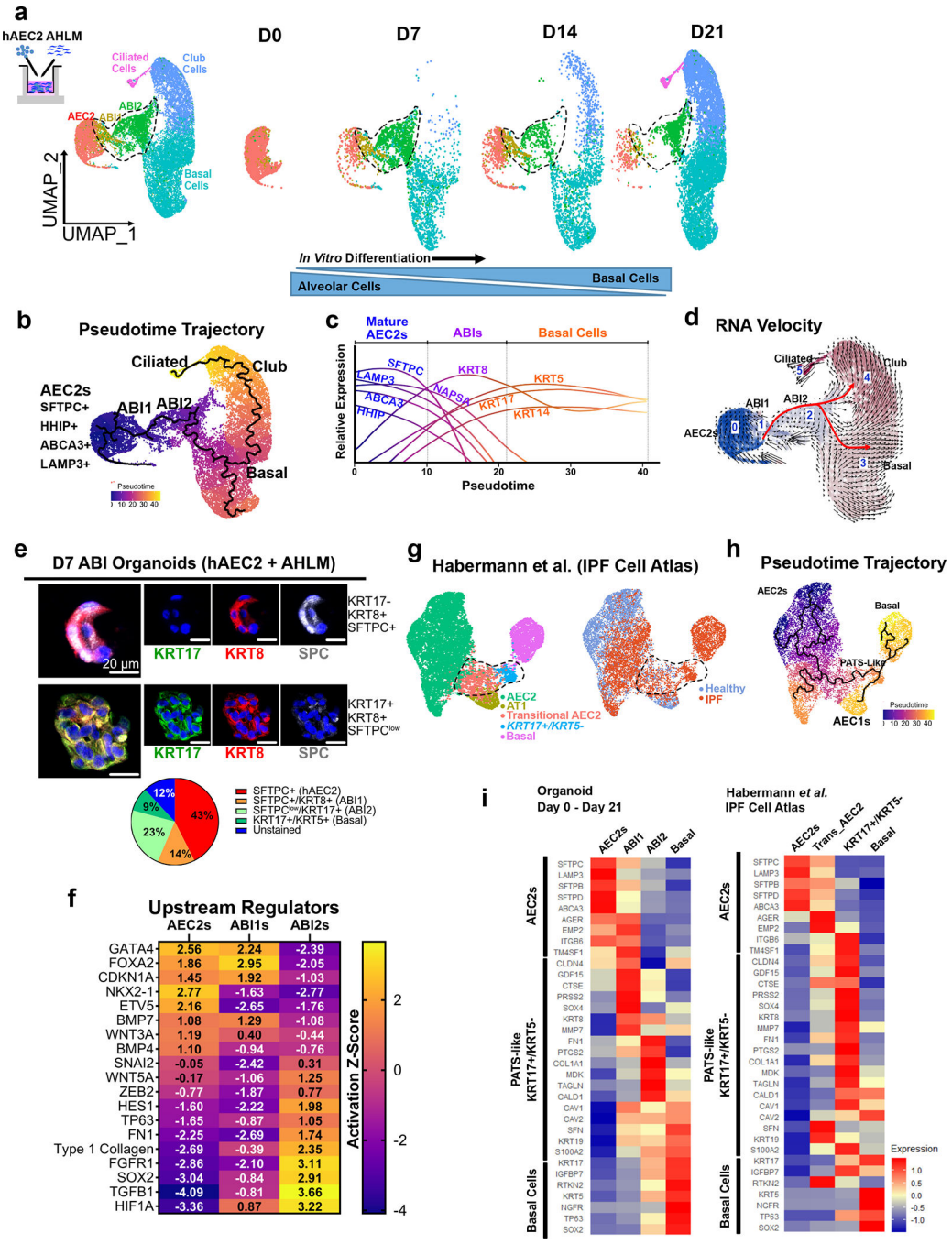

Figure 6: hAEC2 transdifferentiates into KRT5+ basal cells through alveolar-basal intermediate (ABI) cells *in vitro* and *in vivo*

(**a**) scRNA-seq of freshly sorted HTII-280+ hAEC2s (D0) and hAEC2s co-cultured with AHLM at D7, D14, and D21. (**b-d**) Pseudotime ordering of epithelial cells from D0, D7, D14, and D21 organoids identify an hAEC2s → ABIs → Basal → Club → Ciliated cell trajectory based on gene expression levels over pseudotime trajectory that was confirmed on RNA Velocity. (**e**) Immunofluorescence staining of D7 hAEC2+AHLM organoids identify presence of KRT17−/KRT8^{high}/SFTPC+ ABI1 (14%) and KRT17+/

KRT8+/SFTPC^{low} ABI2s (23%) along with SFTPC+ hAEC2s (43%) and KRT17+/KRT5+ basal cell (9%). Representative of n=2 biologically independent experiments performed in technical triplicates each. Data are represented as mean of biological replicates. (**f**) Ingenuity Pathway Analysis of the differentially expressed genes between AEC2s, ABI1, ABI2 identified the upregulation of alveolar signaling (NKX2–1, ETV5) in AEC2s, WNT and BMP signaling in AEC2s and ABI1s and fibrotic/airway signaling pathways (TGFβ1, HES1, extracellular matrix genes, SOX2, and TP63) in ABI2s. (**g,h**) Re-analysis of IPF epithelium from Habermann et al. to include basal cells along with PATS-like cells (encompassing transitional AEC2s and KRT17+/KRT5− cells on UMAP) with pseudotime ordering. (**i**) Heatmaps comparing lineage-specific gene expression of KRT17+/KRT5− basaloid cells in IPF (labeled as PATS-like cells by Kobayashi et al[20]) and ABIs in 3D organoid.

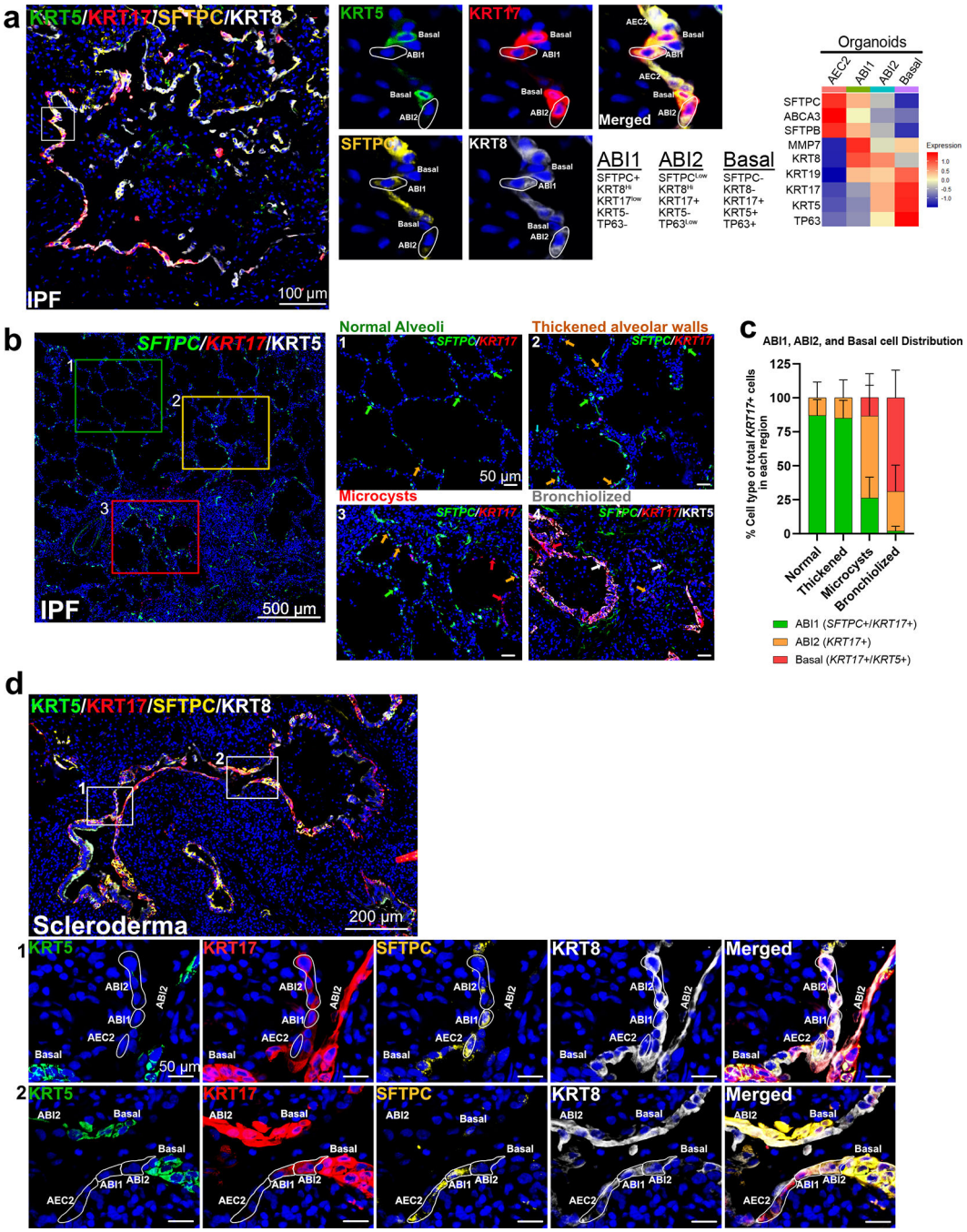

Figure 7: Evidence of hAEC2-to-basal transition through ABIs in severe alveolar injury.

(**a**) Immunostaining of IPF lungs finds hAEC2s (SFTPC+), ABI1 (SFTPC+/KRT17^{low}), ABI2 (SFTPC^{low}/KRT17+/KRT5−), and Basal cells (KRT5+/KRT17+) in the same cystic regions. Heatmap shows average expression of select candidate genes in each cell types in organoids. Representative of n=3 IPF specimens. (**b, c**) *In situ* analysis of IPF lungs identify decreasing frequency of ABI1s (*SFTPC*+/*KRT17*+; orange arrows) and increasing frequency of ABI2s (*SFTPC*−/*KRT17*+/KRT5−; red arrows) and basal cells (*SFTPC*−/*KRT17*+/KRT5+; white arrows) as severity of fibrosis increases. Green arrows indicate

AEC2s (*SFTPC*+/*KRT17*-). Representative of n=6 independent IPF specimens used to define normal, thickened, microcystic, and bronchiolized regions. Each region included at least 4 images taken at 20X from at least three IPF specimens. Data are represented as the average of all the images and error bars are standard deviation. (**d**) Immunostaining of scleroderma lung identifies linear progression from hAEC2s → ABI1→ ABI2 → Basal cell in the same region. Images representative of n=1 scleroderma lung.

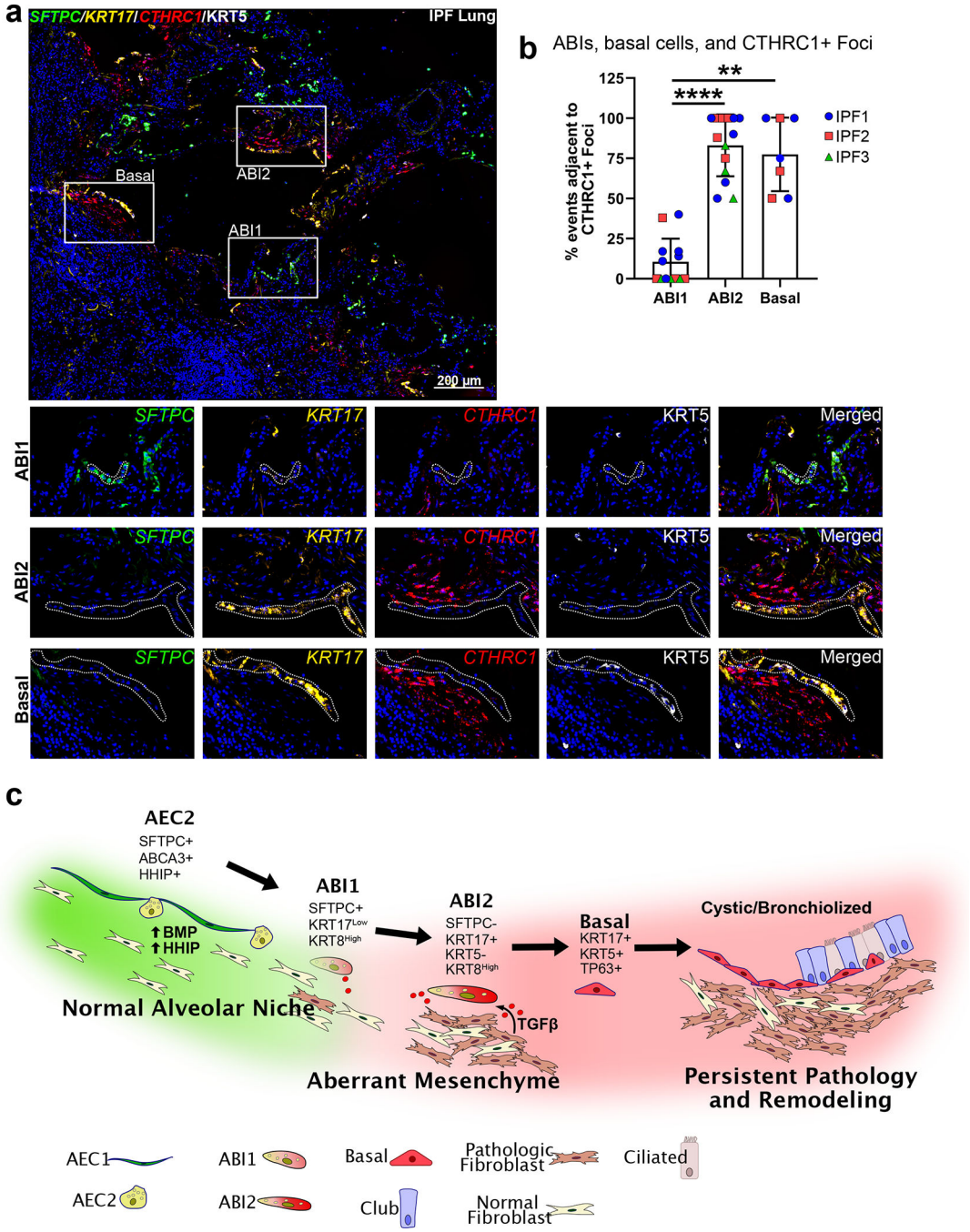

Figure 8: ABIs and basal cells in actively remodeling regions in IPF lungs are adjacent to aberrant CTHRC1^{high} mesenchyme

(**a, b**) RNA *in situ* hybridization was performed for *SFTPC*, *KRT17*, and *CTHRC1* followed by KRT5 protein staining. 83% of ABI2s (*SFTPC*−/*KRT17*+/KRT5−) and 77% of basal cells (*KRT17*+/KRT5+) found in actively remodeling regions were in close proximity to clusters of CTHRC1^{high} fibroblasts. Representative of n=3 independent IPF lungs analyzed. Each dot in **b** represents an average of at least a 3×3 tiled region captured at 20X. In total, 160 images were captured at 20X and counted across three IPF specimens. Data

is represented as mean ± SD. Significance is calculated by one-way ANOVA followed by Kruskal-Wallis test for multiple comparisons. **** $p < 0.0001$, ** $p = 0.0014$. **(c)** Schematic illustrating a transdifferentiation pathway of hAEC2s to metaplastic Basal cells through discrete ABIs and as a likely consequence the accumulation of dysplastic alveolar structures prominent in IPF. Transdifferentiation develops as a function of transition of surrounding mesenchyme from a BMP/Wnt high supportive niche (green) to an aberrant, pro-fibrotic niche comprised of fibroblasts high in anti-BMPs, TGFβ1, and ECM proteins (red). Although the schematic highlights active TGFβ1 deriving from fibroblasts, ABIs are also a prominent source of TGFβ1 activation and signaling (See Fig 6; Kobayashi 2020[20], Strunz et al 2020[19]), likely contributing to the development of aberrant mesenchyme and a pro-fibrotic milieu.